A LONG-TERM SPACE ASTROPHYSICS RESEARCH PROGRAM

THE EVOLUTION OF THE QUASAR CONTINUUM

NASA Grant NAGW-2201

Semiannual Report No. 6

For the Period 1 January 1993 through 30 June 1993

Principal Investigator
Dr. M. Elvis

July 1993

Prepared for:

National Aeronautics and Space Administration
Washington, DC 20546

Smithsonian Institution
Astrophysical Observatory
Cambridge, Massachusetts 02138

The Smithsonian Astrophysical Observatory
is a member of the
Harvard-Smithsonian Center for Astrophysics

The NASA Technical Officer for this grant is G.R. Riegler, Code: SZE, National Aeronautics and Space Administration, Washington, DC 20546.

Harvard-Smithsonian Center for Astrophysics

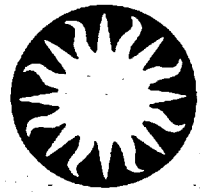

Preprint Series

No. 3626
(Received May 3, 1993)

THE ROSAT SPECTRUM OF 3C351: A WARM ABSORBER IN AN X-RAY 'QUIET' QUASAR?

Fabrizio Fiore, Martin Elvis, Smita Mathur, Belinda J. Wilkes and Jonathan C. McDowell
Harvard-Smithsonian Center for Astrophysics

To appear in
The Astrophysical Journal
September 20, 1993

HARVARD COLLEGE OBSERVATORY SMITHSONIAN ASTROPHYSICAL OBSERVATORY
60 Garden Street, Cambridge, Massachusetts 02138

Center for Astrophysics
Preprint Series No. 3626

THE ROSAT SPECTRUM OF 3C351: A WARM ABSORBER IN AN X-RAY 'QUIET' QUASAR?

Fabrizio Fiore, Martin Elvis, Smita Mathur, Belinda J. Wilkes and Jonathan C. McDowell

Harvard-Smithsonian Center for Astrophysics

60 Garden Street, Cambridge, MA 02138

March 10, 1993

Accepted for publication in The Astrophysical Journal

1993 September 20 issue

Overview

The research program supported by this grant now has great momentum. Numerous papers are in progress, and a strong multi-wavelength observing program is rapidly accumulating data on samples of high redshift quasars across the spectrum.

ROSAT spectra of quasars continue to yield surprises. Of four $z = 3$ quasars with X-ray spectra, three show strong absorption. This contrasts strongly with the situation for luminous AGN at low redshifts where fewer than 1 in 20 show X-ray absorption. A new site for this absorption is probably needed, either around the quasar (e.g. in a cluster cooling flow) or along the line of sight (e.g. in a Damped Lyman-alpha system). The unabsorbed quasar allows limits on the physical conditions in a damped Lyman-alpha cloud to be calculated, and will allow a X-ray Gunn-Peterson test to be applied that will limit the fraction of the closure mass in an intergalactic medium. The X-ray spectral indices of these $z = 3$ quasars show no change from those of similar objects at low z, suggesting that 'short-lifetime' models apply.

Eight other z =3-4 quasars have been detected and their energy distributions from X-rays to Infrared (using new infrared spectrographs) have been compiled. These are now being compared with the low z continua from the 'Atlas of Quasar Energy Distributions' to search for evolutionary changes.

The discovery of a likely warm absorber in 3C351 made recognition of another example simple. Also, modelling of the conditions in the absorber in 3C351 using the OVI absorption line from HST and the high ionization emission lines, suggests that the broad line region is indeed the origin of the warm absorber in this quasar, and by extension, others. Warm absorbers can now be used as a new diagnostic of this region.

The X-ray spectrum of a 'Red Quasar', 3C212, has a cut-off spectrum, which could be fitted by an absorbed power-law, or more remarkably, by an unabsorbed black body. Using our quasi-simultaneous optical data and photoionization modelling we are able to rule out this latter possibility. The long-sought key to understanding red quasars has now been found. (Reddening was earlier ruled out because no 2175Å absorption feature was seen. This is now seen to have been misleading.)

Refereed Papers

A ROSAT Spectrum of 3C351: A Warm Absorber in an X-ray 'Quiet' Quasar? (F. Fiore, M. Elvis, S. Mathur, B.J. Wilkes, and J.C. McDowell), 1993, *Ap.J.*, in press (Sept. 20).

Absorption in ROSAT Spectra of High Redshift Quasars (M. Elvis, F. Fiore, B.J. Wilkes, J.C. McDowell, and J. Bechtold), 1993, *Ap.J.*, in press.

An Atlas of Quasar Energy Distributions. (M. Elvis, B.J. Wilkes, J.C. McDowell, R.P. Green, J. Bechtold, S.P. Willner, M.S. Oey, E. Polomski, and R. Cutri), *Ap.J. Suppl.*, submitted.

X-ray Absorption toward the Red Quasar 3C212 (M. Elvis, F. Fiore, S. Mathur and B.J. Wilkes *Ap.J.*, in preparation.

Infrared to X-ray Spectral Energy Distributions of High Redshift Quasars (J. Bechtold, O. Kuhn, M. Elvis, F. Fiore, B.J. Wilkes, R. Cutri, M. Rieke et al.) 1993, Ap.J., in preparation.

Optical and Ultraviolet constraints on the X-ray warm absorber in 3C351 (S. Mathur, F. Fiore, B.J. Wilkes M. Elvis etal.) 1993, Ap.J., in preparation.

Talks/Presentations Given

F. Fiore:

— GSFC, MD- April: 'ROSAT Results on AGN'

S. Mathur:

— Conference on "Mass Transfer Induced Activity in Galaxies", Louisville KY- April
— 3rd New England Regional Quasar Meeting, Cambridge MA- May: 'AGN Induced Effects in NGC1068'

M. Elvis:

— IAU Symposium on 'Particle Acceleration in Astrophysics', College Park MD- January: 'X-ray Spectra of AGN: A misleading clue'
— Osservatorio di Roma, ITALY- May: 'X-ray Absorption toward z=3 Quasars'
— Istituto Astrofisico di Roma, ITALY- May: 'ROSAT Observations of Extreme AGN'
— 3rd New England Regional Quasar Meeting, Cambridge MA- May: 'X-ray Spectra of High Redshift Quasars'
— AAS meeting- Berkeley CA: 'X-ray Absorption toward High Redshift Quasars'
— Workshop on the Dynamic ISM/IGM- Aspen CO: June

1. "X-ray and 21cm column densities at high Galactic latitudes"
2. "Extended X-ray emission in AGN"
3. "X-ray absorption toward z=3 quasars"

B. Wilkes:

— Invited talk, *Spectral Energy Distributions* at the 3^{rd} annual New England Regional Quasar and Active Galaxies Meeting, May 12^{th} 1993 Cambridge, Massachusetts
— Invited talk, *X-rays and γ-rays from Quasars: a View of the Heart* at the 1^{st} annual Mt. Stromlo and Siding Spring Observatory Symposium, 30^{th} June 1993, Canberra, Australia

Abstract

3C351 is one of the most X-ray quiet radio quasars ($\alpha_{OX} \sim 1.6$). We have observed 3C351 with the ROSAT PSPC and find a complex X-ray spectrum which is not well reproduced by a power law plus low energy cut-off model. Soft excess, partial covering, and 'warm absorber' models can all produce acceptable fits, although only the warm absorber model gives typical values for the high energy continuum slope. The α_{OX} measured by using quasi-simultaneous ROSAT, MMT and HST observations is in the range 1.5-1.6, significantly above the average of 1.37 ($\sigma \sim 0.15$) for a complete sample of 33 3CR quasars. If the soft excess or partial covering models are correct, 3C351 appears X-ray quiet in the PSPC band because it has an extremely steep or flat intrinsic high energy spectral slope. However, if the warm absorber model is correct, the quasar is intrinsically X-ray quiet - the normalization of the intrinsic (unabsorbed) X-ray emission is unusually low relative to the optical luminosity. We investigate the properties of our warm absorber model in some detail. The apparently complicated behaviour of the fit parameters may be understood by considering the effects of changing absorbing column and ionization parameter on intrinsic power law spectra of different slopes.

Subject headings: Quasars - X-ray: Spectra

1 INTRODUCTION

Most quasars are X-ray sources, but the range of their X-ray output relative to the optical (or ultraviolet or infrared) is large, covering a range of $\sim$ 400 (Zamorani *et al.* 1981, Tananbaum *et al.* 1986). While Avni and Tananbaum (1986) showed that only a minority (<8%) of all quasars could be 'X-ray silent', they also found that most quasars are relatively X-ray quiet. In terms of the commonly used parameter α_{OX} (the two point spectral index between the optical, 2500Å and X-ray, 2 keV) this distribution covers the range from α_{OX} $\sim$0.9 to $\sim$2 (Tananbaum *et al.* 1986, Elvis and Fabbiano 1984, Makino *et al.* 1989).

What is the cause of this 'X-ray quietness'? Extreme spectra, either flat (or absorbed), or steep could remove photons from the observed band without affecting the X-ray flux; a low normalization to the spectra is a possibility, so that the same process is 400 times less efficient at generating X-rays in some quasars as in others; and, since observations establishing L_{opt} and L_X have not been made simultaneously, large amplitude X-ray variability by a factor $\sim$ 400 in the few years between the optical and X-ray observations, even though variations of only factor $\sim$ 2 are typical in the optical, could produce a range of X-ray loudness. Each of these explanations would involve extreme physics, and most imply unusual spectral properties.

X-ray quietness is less extreme among radio-loud quasars. A complete sample of 3CR quasars (f(178MHz)>9Jy and V<18) was studied in X-rays by Tananbaum *et al.* (1983) who detected all 33 objects. They found a maximum α_{OX} of 1.67. 3C351 (z=0.371, Veron-Cetty and Veron 1991) is one of the most X-ray quiet radio quasars (α_{OX}=1.6, Tananbaum *et al.* 1986). It is also one of the very few X-ray quiet quasars with an X-ray flux sufficient to obtain a spectrum with *Einstein* or ROSAT (1.0×10^{-12} erg s^{-1} cm^{-2}, 0.5-4.5 keV, assuming $\alpha_E = 0.5$ and Galactic absorption, Tananbaum *et al.* 1986). 3C351 has a flat X-ray spectrum in the *Einstein* IPC (Elvis *et al.* 1993). On the other hand 3C351 qualified securely as an 'ultra soft source' in one of the 12 IPC observations (Cordova *et al.* 1992). Something unusual seems to be happening in the X-ray spectrum of 3C351.

The radio structure of 3C351 is double-lobed with most of the emission concentrated in one lobe (Leahy and Perley 1991). The total flux at 5 GHz is $\sim$ 1.2 Jy and the fraction of flux density contained in the compact core is very low: 0.65 % at 6 cm (Kellermann *et al.* 1989). In the view of Unified Models (Orr and Browne 1982, Barthel 1989), the dominance of the core is a measure of the inclination of the radio axis to the line of sight: core dominated quasars are viewed with their radio axis end-on and the flux density amplified due to the Doppler effect (e.g. Blandford and Kõnigl 1979); lobe-dominated quasars are viewed edge-on. Thus 3C351, with its weak core, may be close to edge-on. This may be related to its X-ray quietness because the X-ray flux could be linked with the radio flux and/or because of the X-ray flux could be blocked by intervening matter along the line of sight.

Before the launch of ROSAT (Trümper 1983) significant intrinsic absorption has been discovered only in two luminous quasars, MR2251-178 (Halpern 1984, Pan, Stewart and Pounds 1990) and NRAO 140 (Marscher 1988, Turner *et al.* 1991). In the first case the absorption is not produced by neutral gas, but by partially ionized "warm" material (Halpern 1984, Pan, Stewart and Pounds 1990). A signature of such material is a flattening of the spectrum above the oxygen K-edge at ~1 keV, and an excess flux below the edge, at ~0.25 keV, where the ionized lighter elements become transparent. There is a possibility that warm absorbers could reduce the X-ray loudness of an AGN without totally removing soft photons and rendering it undetectable. The ROSAT PSPC (Position Sensitive Proportional Counter, Pfefferman *et al.* 1987) bandpass (0.1-2.5 keV) is particularly useful for studying the effects of soft X-ray absorption. Furthermore, its improved energy resolution and signal-to-noise with respect to the Imaging Proportional Counter on Board the *Einstein* satellite will allow the investigation of the details of such complex absorption systems.

We observed 3C351 with the PSPC between October 28 and 30 1991 for a total livetime of 13068 s. We find a complex X-ray spectrum which suggests that we view the quasar through a partially ionized region of gas, a warm absorber.

2 OBSERVATIONS AND DATA ANALYSIS.

The distribution of the X-rays from 3C351 was consistent with the 25″ FWHM of PSPC point response function and the centroid of the distribution is only 8″.7 from the optical position (R.A. 17h 04m 03.4s, dec. 60d 48m 31.1s, B1950) an offset typical of ROSAT pointings. Source counts were extracted from within a 2′ radius around the source centroid (containing at least 95% of the source counts, Turner and George 1992). The background was estimated within an annulus of inner and outer radii 2.′5 and 5′ respectively. Within 6′ of the 3C351 centroid five weak sources are detected. Circular regions of radius 1′.5 centered on these sources were then excluded from the analysis. The distribution of the counts from 3C351 falls to the background level at a radius of ~ 1′.5. The total net source counts within 2′ are ~ 1420 and the estimated background counts are ~ 340. During the observation, spanning over two days, the variations of the 0.1-2.45 keV source intensity were smaller than ≈ 40% and the count rate is consistent with a value of 0.106±0.003 PSPC ct s^{-1} at the 5 % confidence level. Assuming $\alpha_E = 0.5$ and Galactic absorption as in Tananbaum *et al.* (1986) this corresponds to a 0.5-4.5 keV flux of 1.25×10^{-12} erg $s^{-1}cm^{-2}$, similar to the IPC value. The 34 energy channels used by MPE SASS pipeline processing are used in the following analysis.

2.1 Systematic Error Estimate

The good temporal and spatial gain stability of the PSPC makes it possible to achieve a good calibration of this imaging proportional counter (ROSAT news No 10, 1992). Nevertheless, there are residual systematic uncertainties in the knowledge

of the resolution matrix of order a few percent. In particular the following systematic features have been found in the residuals of PSPC spectral fits of high signal to noise data (ROSAT news No. 10, 1992): (a) a systematic deficiency of measured counts above the carbon edge (around 0.4 keV) with associated excesses between 0.2-0.4 keV and 0.7-0.9 keV; (b) an excess of measured counts above 2 keV.

To quantify the magnitude of the above systematic features we analyzed the spectrum of the quasar PG1426+015 (Wilkes *et al.* 1993), which is about ten times brighter than 3C351 in soft X-rays, and was observed by the PSPC on July 1990 for a total livetime of 6485 s and a 0.1-2.45 keV count rate of 1.4 ct s^{-1}. The pulse height spectrum is plotted in Fig. 1 along with the best fitting power law, reduced at low energy by Galactic absorption. The fit was performed using the March 1992 version of the PSPC response matrix installed in the SASS processing system (DRM_9). The value of the reduced χ^2 (1.28 for 30 degrees of freedom, dof, corresponding to a 14% probability of finding a greater χ^2 by chance) indicates that the model is an adequate representation of the data. The best fit values for the spectral index, the 0.1-2.45 unabsorbed flux, and absorbing column were 1.54 ± 0.13, $3.2 \pm 0.1 \times 10^{-11}$ erg cm^{-2}, s^{-1}, and $2.6 \pm 0.3 \times 10^{20}$ cm^{-2} (consistent with the Galactic value of 2.64×10^{20} cm^{-2}), respectively. In the lower panels we plot the residuals after the subtraction of the model from the data both as a number of σ and as a fraction of the source net counts in each channel. A deficiency of the measured counts is seen around 0.4 keV (channels 10-12) as well as an excess around 0.3 keV (channels 8-9). The magnitude of these features is small, of the order of 1 σ per channel, or about 5% of the source net counts per channel. A small excess of the measured counts is also present above 2 keV but in that region the statistics are not good enough to obtain useful information on the magnitude of the systematic error.

These deviations form an upper limit to the systematic errors on the PSPC response matrix since the quasar may itself contain real spectral features more complex than a power law. The magnitude of the features is quite negligible compared with the statistical errors per channel in the spectrum of 3C351, which range from 12 to 31 % of the net source counts in those channels.

As a further test we analyzed the data of the BL LAC object 1E1704.9+6047 (Gioia *et al.* 1990), which is in the same ROSAT field of 3C351 at just 7′ from the quasar. Source counts were extracted from within 2′.5 around the source centroid and the background was estimated within an annulus of inner and outer radii 3′ and 5.5′, respectively. The total net source counts were $\sim$ 1030, comparable with those of 3C351. The spectrum of 1E1704.9+6047 was fitted to a simple power law plus low energy absorption. The reduced χ^2 is 1.32 (28 dof, corresponding to a 12% probability) and the residuals do not present strong features at any energy. The column density ($N_H = 2.3 \pm 0.3 \times 10^{20}$ cm^{-2}) is compatible with the Galactic value along the line of sight of $2.26 \pm 0.10 \times 10^{20}$ cm^{-2} (Elvis, Lockman and Wilkes 1989). The spectral index is 1.33 ± 0.25 and the 0.1-2.45 keV unabsorbed flux is

$1.4 \pm 0.2 \times 10^{-12}$ erg cm^{-2} s^{-1}.

In the following analysis we include a systematic error of 2 % (as suggested in ROSAT news No 10, 1992) by adding it in quadrative to the statistical error in each channel. The fits are performed over the 0.1-2.45 keV energy range (channels 2-34). The errors represent the 68 % confidence interval.

3 RESULTS.

3.1 Simple Power Law

We first attempted a fit to the 3C351 ROSAT spectrum of a simple power law model reduced at low energies by absorption from a neutral gas with solar abundance (using cross-sections from Morrison and McCammon 1983; we designate this as our model 1). The results of the fit are shown in Fig. 2 and given in Table 1 where the errors are given for two interesting parameters following the prescription of Lampton, Margon and Bowyer (1976). The energy spectral index is $\alpha_E = 0.47 \pm 0.16$, rather flat for a lobe-dominated quasar and similar to that found using the *Einstein* IPC data by Elvis *et al.* (1993). The column density is $N_H = (0.39 \pm 0.25) \times 10^{20}$ cm^{-2}, significantly lower than the Galactic value along the line of sight of 2.26×10^{20} cm^{-2} (Elvis, Lockman and Wilkes 1989). The χ^2_r of 2.18 for 28 dof, is unacceptably large (probability of 3×10^{-4}). The poor quality of the fit is illustrated by the residuals plotted in the lower panel of Figure 2. We see a clear 36 % deficit in the counts measured between 0.6 and 0.9 keV (channels 14-19); a $\sim$ 15% excess between 0.2 and 0.4 keV (channels 5-9); and an excess above 1 keV. The strong deficit between 0.6 and 0.9 keV is significant at $\sim 10\sigma$. This deficit cannot be explained in terms of a systematic effect in the resolution matrix, since at those energies the residuals of PG1426+015 are flat to 5% ($\pm 1\sigma$, see above, Figure 1), while the observed deficit in 3C351 is some 2.5 times larger. [1] A fit of the same model with N_H fixed at the Galactic value gives a χ^2_r of 4.08 (29 dof), a rather steep power law slope, $\alpha_E = 1.31 \pm 0.05$, and qualitatively similar residuals. Fits with a single thermal component such as a black body, a thermal bremsstrahlung and a Raymond-Smith (1977) model, all give χ^2 significantly higher than model 1.

We must therefore investigate more complex models for 3C351. Model 1 can be modified by changing either the emission law, or the absorption law, or both. We tried three modifications.

3.2 Soft Component

A soft component was added to the emission law, as suggested by the report of an excess in the 0.1-0.5 keV band by Cordova *et al.* (1992) and by the measure of

[1] A fit performed with the more accurate resolution matrix released in January 1993 (DRM_36_1) confirms this conclusion: the residuals appear qualitatively similar to those in Fig. 2 and the χ^2 for a simple power law model is slightly worse than that in Table 1.

an N_H much lower than the Galactic value in model 1. Parameterizing the excess as a steep power law we obtain the results given in Table 1 and the residuals shown in Fig. 3a. The χ^2_τ is now acceptable (1.03 for 26 dof) and the improvement in its value is significant at >> 99.9% confidence level, using the F-test(F=33.3; a significant improvement at the 99.99 % level requires F=13.74, Abramowitz and Stegun 1964). The N_H of $4.8 \pm 3.0 \times 10^{20}$ cm^{-2} is now compatable with the Galactic line of sight value. The spectral index of the soft power law is poorly constrained. The hard power law, however is well determined at $\alpha_E = -0.04^{+0.34}_{-0.25}$ (errors for three interesting parameters). Such a flat spectral index is very unusual in AGN, especially in lobe-dominated quasars (Shastri *et al.* 1993). Similar results were obtained parameterizing the soft excess as a black body (the temperature is again poorly constrained, $T \lesssim 0.08$ keV).

3.3 Partial Covering

The second modification is to make a partial covering model for the absorption law, so that only a fraction F_C of the source has this absorption applied to it. The Galactic absorption remains fixed at the Elvis *et al.* (1989) value. The results are again given in Table 1 and the residuals are shown in Fig. 3b. The fit is again very good ($\chi^2_\tau = 0.97$ for 27 dof) and the improvement in χ^2 with respect to the fit with model 1 is highly significant. The large N_H measured here, $(2.0^{+0.7}_{-0.4}) \times 10^{22}$ cm^{-2} (errors for 3 interesting parameters) takes into account the reduction of counts just below 1 keV seen in Fig. 2, while the large number of counts observed between 0.1 and 0.6 keV is explained by the unobscured part of the source. The spectral index turns out now to be very steep, $\alpha_E = 2.12^{+0.42}_{-0.31}$. Quasars with such steep α_E have been observed in soft X-rays (e.g. PG1211+143, Elvis *et al.* 1991; see also Elvis, Wilkes and McDowell 1990 for a review), but none of them have high intrinsic absorption detected as well.

3.4 Warm Absorber

Since these simple modifications gave unusual continuum slopes we also investigated a third modification to the absorber in model 1, a "warm" absorber (Halpern 1984). This model leaves the ionization level of the absorber free to vary, as discussed by Krolik and Kallman (1984). When the ionization parameter, defined as

$$U = \frac{Q}{4\pi r^2 n_H c},$$

where Q is the total number of ionizing photons per second and n_H is the total number density of Hydrogen, is very low only the ground state and low ionization states of the elements responsible for the absorption of X-rays are significantly populated and the assumption of a completely neutral absorber is a good approximation of the actual situation. When the ionization parameter is very high most of the elements from H to O are completely ionized and, at least in the 0.1-2.5 keV energy range, the

assumption of no intrinsic absorption is a good one. When, however, not all the C, N, O, and Ne are completely ionized, they can give rise to significant absorption above $\sim$ 0.3 keV even if H and He are completely ionized. In particular, if He is completely ionized while the heavier elements are not, the gas is transparent below $\sim$ 0.3 keV and almost opaque above this energy. These warm absorbers give rise to edge structures in the transmitted spectrum with the Oxygen K-edges (0.54-0.87 keV) being the most prominent. Since a deficit between 0.6 and 0.9 keV is the largest feature in the residuals in Fig. 2, models which include the possibility of an absorption edge are promising.

3.4.1 Simple Power Law plus Edge

As a first, simplified, investigation we parameterize such a model assuming that the incident power law is absorbed by neutral gas with column density N_{H1} above an energy E_0 while below this energy it is absorbed only by the Galactic N_H. The results of this fit are again listed in Table 1 and are shown in Fig. 3c. The χ^2_τ (1.23 for 27 dof) is again good, though marginally higher than the previous two cases. The spectral index is $\alpha_E = 0.96^{+0.15}_{-0.10}$(errors for three interesting parameters). This continuum slope is consistent with those of other lobe-dominated quasars (Shastri *et al.* 1993). The rest frame energy E_0 of the edge is $0.68^{+0.1}_{-0.2}$ keV (errors for three interesting parameters). K-edges of ions of Carbon, Nitrogen, and Oxygen are present in this energy interval (Band *et al.* 1990). The less conservative errors for just one interesting parameter reduce the confidence interval for the edge energy to 0.58-0.76 keV: only K-edges of N VII and O IV, O V, O VI and O VII are present in this interval.

The 'reasonable' spectral slope obtained with the above model suggests that a warm absorber may be appropriate. The above model is however not physical and therefore the next step was the construction of a full warm absorber model using a photoionization code.

3.4.2 Construction of a Physical Warm Absorber

To construct a warm absorber model only three ingredients are necessary: a) the relative abundance of each ion of the elements responsible for the X-ray absorption in the studied energy range, b) the elemental abundances, and c) the cross-section for photoelectric absorption of each ion. The relative abundance of ions is a function of: the number density of the gas; its column density; and of the shape and intensity of the ionizing continuum. The photoionization code CLOUDY (version 80.06, Ferland 1991) was used to determine the relative abundances of all ions of H, He, C, N, O, Ne, Mg, Al, Si, S, Ar, Ca, and Fe (a total of 153 ions) for a grid of values of N_H ($10^{21} \lesssim N_H \lesssim 10^{23}$ cm^{-2}), a series of simple ionizing continua and a grid of values of the ionization parameter U (which is the dimensionless ratio between the number of ionizing photons and the gas density and therefore represents the normalization of the incident continuum, $0.04 \lesssim U \lesssim 0.25$). The abundances relative to Hydrogen of each

element were fixed at the solar value (Grevesse and Anders 1989). The continuum was parameterized as a power-law of slope α_E with low and high energy cut-offs. The resulting ion abundances are insensitive to the low energy cut-off, provided that it is shortward of $\sim$ 100 microns. In the following we fixed the low energy cut-off at 10 microns, but the abundances do not differ qualitatively from those obtained with cut-offs from 100 microns to 912 Å . The ion abundances depend slightly on the position of the high energy cut-off. We tried cut-offs at 50 keV and 5 MeV. The result is a slightly flatter emergent continuum when the cut-off is at 5 MeV ($\Delta\alpha_E \sim 0.2$). In the following we present the results fixing the high energy cut-off at 5 MeV. The ion abundances do depend strongly on the slope of the incident continuum. We therefore computed them for a grid of values of α_E from 0.3 to 1.2. The abundances do not depend significantly on the volume density of the gas, provided that it is between 10^8 and 10^{11} cm^{-3}. We fix it at 10^9 cm^{-3}.

In conclusion, all the information obtained using CLOUDY is contained in a four-dimensional matrix (153 (ions) x N (values of α_E), x M (values of U) x L (values of N_H)). We used N=10, M=15 and L=20. This model of warm absorbers has therefore 3 free parameters: the slope of the ionizing continuum, α_E, the ionization parameter, U, and the gas column density, N_H

At present there are no universally accepted values for the photoionization cross-sections. The uncertainties are particularly large for the cross-sections for removal of the outer electrons of atoms. To understand to which extent the uncertainty in the cross-sections can affect the evaluation of the parameters of the warm absorber we used two different sets of cross-sections. The first was extracted from CLOUDY and consists of unpublished values by C. Mendoza (Ferland 1991). The second is a compilation by A. Fazzolari and G. C. Perola constructed by using the results of Reilman and Manson (1979), and by using the formulae of Band *et al.* (1990) to find the cross-sections of each ion at energies greater than the K-edge. The position of the K absorption edges are from Band *et al.* (1990); those of the L and M edges of neutral atoms from Henke *et al.* (1982). All this information is contained in a two-dimensional matrix (479 (energies) x 153 (ions)).

3.4.3 Fitting the Warm Absorber model

The opacity of the gas as a function of the energy and for each given value of α_E, U and N_H is found by interpolating linearly over the matrix of the ion abundances and then multiplying the result by the matrix of the cross-sections. The discrepancies between interpolated abundances and "true" ones (those found running CLOUDY) are always smaller than 10 %. In the following we present the results obtained using the CLOUDY cross-sections and discuss the differences with those obtained using the Fazzolari and Perola cross-sections.

Since nothing is known about the location of X-ray warm absorbers, and to limit as much as possible the number of free parameters, in the following analysis

we adopted the simplest possible geometry, i.e. a plane parallel geometry (thickness of the cloud much smaller than the distance between the cloud and the source of the X-ray continuum), where a single cloud covers completely and uniformly the continuum source. The "geometric" covering factor of the cloud (i.e. the fraction of the source along the line of sight covered by the source) is therefore 1 while the "radiative" covering factor (as defined by Ferland 1991, $f_c = \Omega/4\pi$), is very small and corresponds to an open geometry. The redshift of the warm absorber is fixed at 0.371. A further neutral absorber, of density fixed to the Elvis *et al.* (1989) Galactic value and redshift zero, covers the source.

The χ^2_r obtained by fitting the warm absorber model to the data with all the parameters free is good, 1.06 for 27 dof, but the uncertainties on α_E, U and N_H are large. This is because the moderate energy resolution of the PSPC and the complexity of the model produce a strong correlation between the three parameters. In other words, many models with different values of α_E, N_H and U are able to reproduce the observed spectrum. In particular, the χ^2 is rather insensitive to the value of α_E. We therefore repeated the fit by fixing α_E at a set of values of α_E spanning the range commonly observed in quasars X-ray spectra (Wilkes and Elvis 1987, Williams *et al.* 1992), namely 0.5, 0.6, 0.7, 0.9 and 1.1. The χ^2 are always very good. The results of this series of fits are in Table 1, errors for two interesting parameters, and the case of $\alpha_E = 0.9$ is shown in Fig. 4a. In Fig. 4b the transmitted continuum corresponding to this case is shown. The prominent absorption edge is due to O VII at 0.74 keV. The low energy absorption is due to residual He opacity (in this model the relative abundance of He and He^+ is $\sim 2 \times 10^{-7}$ and 0.01 respectively). The 68 %, 90 % and 99 % contours of χ^2 as a function of U and N_H for the fits with the first four values of α_E are shown in Fig. 5 (the contours for the fit with $\alpha_E = 1.1$ are similar to those for the fit with $\alpha_E = 0.9$ but centered at U=0.22). The contours look quite different in the four cases and the behaviour of warm absorber models as U and N_H are changed appears quite complex. We have looked at these dependencies in some detail and, since they have not been widely discussed in literature, we show how they can be understood in a reasonably intuitive manner in the Appendix.

The results obtained using the Fazzolari and Perola cross-sections are similar concerning the χ^2 but the best fit values of U and N_H are shifted systematically of $\sim$ 20% towards lower values. This is the due to the fact that total cross-section computed with the Fazzolari and Perola compilation is generally about 50 % greater then the CLOUDY total cross-sections in the keV region. Elsewhere the two total cross-sections are generally within 15-20 % one to the other.

4 DISCUSSION.

The ROSAT PSPC observation has revealed that the 0.1-2.4 keV spectrum of 3C351 is complex and cannot be represented by a simple absorbed power law. As discussed in the previous section three different modifications of the simple power

law model are able to reproduce this complex spectrum within the limited energy resolution of the PSPC (about 0.5 keV at 1 keV). Each of the models can explain the results obtained with the IPC where the source was found with a flat spectrum (Elvis *et al.* 1993) during a long (livetime of 33100 s) observation. In all three models the observed spectrum is flat between $\sim$ 0.6 and 2.5 keV and steepens significantly to lower energies, while the intrinsic, emitted, spectra differ strongly.

Two of the models require however unusual conditions: in the two power law model the spectral index of the harder power law is unusually flat for an AGN, especially for a lobe-dominated quasar (Shastri *et al.* 1993); in the partial covering model the spectral index is very steep, $\alpha_E \sim 2$, similar to that measured in an extreme object like PG1211+143 (Elvis *et al.* 1991). The partial covering model also requires a column density of $\sim 10^{22}$ cm^{-2}, covering 90% of the source to reduce the counts below 1 keV. None of the known "soft X-ray quasars" (Elvis, Wilkes and McDowell 1990) has an intrinsic column density of this magnitude. On the other hand, the warm absorber model provides a good fit for values of α_E spanning the range commonly observed in quasar X-ray spectra (Wilkes and Elvis 1987, Williams *et al.* 1992).

Unlike the warm absorber model, the two power law model and the partial covering model models have been extensively used and discussed in previous studies of AGN X-ray spectra. While not excluding these two models, below we will therefore discuss on a deeper level of detail the implications of the warm absorber model. First we discuss the implications of this observation for the 'X-ray quietness' issue.

4.1 X-ray quietness

Our observation of 3C351 allows strong constraints to be placed on the origin of X-ray quietness. In the past measurements of X-ray/optical ratios have been compromised by the possibility of variability between the non-simultaneous multi-wavelength observations. In the optical 3C351 is quite bright (B $\approx$ 15.9) and mildly variable. Angione (1973) and Grandi and Tifft (1974) report variations of a factor $\sim$ 2 on timescales of 5-10 years. To avoid the problem of variability we observed 3C351 in the optical nearly simultaneously with the ROSAT observation. The details of the optical observations, performed with the MMT, will be presented elsewhere (Mathur *et al.* 1993). By a fortunate coincidence 3C351 was also observed in the UV by HST just one week before ROSAT (Bahcall *et al.* 1992). From these nearly simultaneous optical and UV observations it is possible to estimate the 2500 Å source flux during October 1991 to be 4.1×10^{-15} erg cm^{-2} s^{-1} Å $^{-1}$. α_{OX} can therefore be estimated for the four models described in the previous section (see Table 2, which also contains the unabsorbed 0.1-2.45 keV flux for each model).

We see that in the simple power law model and in the partial covering model α_{OX} is $\sim$ 1.6, consistent with the finding of Tananbaum *et al.* (1986), while it is significantly lower both in the two power law model, 1.52, and in the warm absorber model, 1.54. The mean α_{OX} found by Tananbaum *et al.* (1983) by analyzing a

complete sample of 33 3CR quasars is 1.37 with a standard deviation of 0.15. For each quasar α_{OX} was computed assuming $\alpha_E = 0.5$ and Galactic absorption. The peculiar flatness of the spectrum of 3C351 in the "keV" region (either because intrinsically so or because of intrinsic absorption) can explain about 35 % (two power law model), or 25 % (warm absorber model) of the difference between the mean α_{OX} and the 3C351 α_{OX} when the Tananbaum *et al.* (1983) prescription is adopted.

Since our measurement of α_{OX} for 3C351 was obtained with quasi-simultaneous optical, UV and X-ray observations, we can use it to rule out several possibilities for explaining X-ray quietness. Extreme variability is not allowed. Absorption is already corrected for in Table 2 and so, while it can reduce the spread in α_{OX} somewhat, it does not explain the entire range. Extremely steep or flat intrinsic spectra are possible if the partial covering or soft excess models are correct. The warm absorber model suggests, although we have only one case, that the α_{OX} distribution for quasars does have a real width, which is due to a range of intrinsic X-ray normalizations relative to the optical of sources with similar spectra. This intrinsic width, however, is probably somewhat smaller than that estimated by Tananbaum *et al.* (1983), due to a contribution from absorption.

4.2 Warm Absorber Models

Warm absorbers have been invoked previously to explain the X-ray spectra of AGN and quasars: MR2251-178 (Halpern 1984, Pan, Stewart and Pounds 1990); MCG-6-30-15 (Nandra, Pounds and Stewart 1990, Nandra and Pounds 1992); NGC 4051 (Fiore *et al.* 1992); NGC 6814 (Turner *et al.* 1992). For MCG-6-30-15 the evidence for a warm absorber comes from the detection of an edge-like structure in a ROSAT spectrum (Nandra and Pounds 1992). These authors fitted to the data a simple power law plus edge model similar to that discussed in §3.4.1. They found a somewhat higher edge energy (0.825 ± 0.017 keV), suggesting a higher value for the ionization parameter than in the present case. Apart from MCG-6-30-15 and 3C351 evidence for warm absorbers is mostly less direct. This is because of insufficient energy resolution below 1 keV where most of the absorption edges are located. MR2251-178 is however particularly interesting because its X-ray luminosity is similar to that of 3C351 and is the highest among the above sources. The variable absorption in MR2251-178 correlates with the X-ray luminosity as predicted by warm absorber models, since the opacity of the absorber is critically balanced against the incoming ionizing continuum and changes strongly in response to relatively small variations in that continuum.

The interpretation of the complex soft X-ray spectrum of 3C351 in terms of an ionized absorber is not unique, because of the limited energy resolution of the PSPC. Observations of the source above 2 keV with good signal to noise ratio, as it will be possible to perform with *Asuka*, would constrain the X-ray slope and therefore would discriminate among the three model discussed in the previous section.

Another crucial test for the warm absorber model would be observations of large amplitude variations (a factor two or more) since this model makes stringent predictions about the changes in soft X-ray opacity at different energies in response to variations in the ionizing continuum. Unfortunately during the three days of the ROSAT observation the source showed no variations larger than $\sim 40\%$. Factor of two variations are present in the 0.16-3.5 keV light curve of the twelve IPC observations (Cordova *et al.* 1992, see their Figure 6 and Table 3). The amplitude of the variations seems to be different in their three bands (0.16-0.56 keV, 0.56-1.08 keV and 1.08-3.5 keV) thus suggesting the existence of spectral variability, but no clear correlations exist among the three bands. The statistics are however so poor that no definite conclusion can be drawn. Future observations can decisively test the warm absorber model in this quasar.

The confidence intervals for U and N_H obtained in §3.4.3 for normal values of the spectral index are reasonably narrow. In particular, U is limited to the range 0.1-0.2, with the lower limit being particularly stringent, and N_H to the range $(1-5)\times10^{22}$ cm^{-2}. These values depend, however, on the particular shape adopted for the ionizing continuum. Changing the shape would result in a modification of the best fit U, since the ionization parameter can be considered as the normalization of the 0.0136-5000 keV ionizing continuum. Furthermore, as pointed out recently by Netzer (1993), the ionized gas will emit in the X-ray band both lines and continua, and will reflect towards the observer part of the incident continuum. These components might reduce the depth of the Oxygen edges and therefore the best fit values for the ionization parameter and column density obtained with a model which does not include such features would be lower then the actual U and N_H.

The reduction of the depth of the Oxygen edges depends on the intensity of the emitted and reflected radiation in the 0.5-1 keV region, which in turn depends on the geometry of the gas (i.e. on the covering factor) and on the column density and the ionization parameter. In particular, the reflected component varies greatly with f_c , being zero when the covering factor is 0 (as for a single cloud along the line of sight, i.e. the warm absorber model in §3.4.3), and reaching a maximum when the covering factor is 0.5 (Netzer 1993). The intensity of the reflected component varies also with the energy and it has a broad minimum around the energies of the O VII and O VIII edges (Netzer 1993). Therefore, even for small but non-zero covering factors, reflection should not weaken the Oxygen edges significantly. Also the intensity of the continuum and line emission depends greatly on the geometry adopted. The intensity is smallest when a single cloud of dimension larger than the source of the ionizing radiation covers completely the line of sight. The intensity of the continuum and line emission varies greatly with U and N_H, increasing rapidly going towards large N_H (the order of 10^{23} cm^{-2}) and large U ($U \gtrsim 1$). For the best fit value obtained for U and N_H in §3.4.3 the strongest emission lines in the ROSAT band are at 0.574 keV (O VII) and 0.654 keV (O VIII and the recombination line from fully stripped ions). The

detection of these individual lines with instruments having good energy resolution, such as the CCDs that will be on board of *Asuka*, JET-X and XMM (although it is not clear whether these CCDs will have enough sensitivity at these low energies), and the calorimeter that will be on board AXAF-S would permit constraints to be placed on the geometry of the gas. Furthermore, since for a given value of N_H the relative intensity of these lines changes strongly as a function of U, measuring their ratio would provide a detailed diagnostic of the warm gas.

Keeping in mind the limitations discussed above on the constraints obtained in §3.4.3 on U and N_H, we can tentatively estimate the physical thickness of the warm absorber and its distance from the central source, with only the volume density as a free parameter. The geometric depth of the region containing the ionized gas is

$$\Delta R = 10^{13}(\frac{N_H}{10^{22}cm^{-2}})\ (\frac{n_H}{10^9\mathrm{cm}^{-3}})^{-1}\mathrm{cm}$$

where n_H is the total number density of Hydrogen. From the definition of ionization parameter, and by using the best fit parameters for the case $\alpha_E = 0.9$ to find $Q \approx 3 \times 10^{55}$ ph s^{-1}, it follows that the distance of the gas from the source of the continuum, r, is

$$r = 9 \times 10^{17}(\frac{U}{0.1})^{-1/2}\ (\frac{n_H}{10^9\mathrm{cm}^{-3}})^{-1/2}\ \mathrm{cm},$$

assuming isotropic emission. This is similar in size to the Broad Line Region of quasars of this luminosity, and much larger than expected accretion disk dimensions (for $10^8 \lesssim n_H \lesssim 10^{11}$). Such a large dimension for the region containing the warm gas is however inconsistent with the assumption of a simple power law ionizing continuum of slope $\lesssim 1$, since most of the optical-UV radiation should be generated well within the central parsec and the α_{OX} of this quasar is in the range 1.5-1.6. Since the ionization structure of Oxygen is mainly determined by the number of ionizing photons around 0.5 keV the addition to the ionizing continuum of a steep optical-UV flux to the X-ray power law, should change only the normalization of the ionizing continuum (i.e. the ionization parameter). The value of U which gives rise to similar relative abundances of Oxygen ions would then be higher than in the simple power law case. In fact assuming a photoionizing continuum consisting of a broken power law, with an X-ray slope of 1 and an UV-soft X-ray slope of 4 produces again a good fit while giving U in the range 1-2.5 (Mathur *et al.* 1993).

The association of the warm absorber with the BLR could also be tested for consistency using the predicted intensities for the optical and UV emission lines that must arise from the absorbing material. The detailed investigation of a self-consistent warm absorber model able to explain the broad-band optical-UV and X-ray continuum and line emission is however beyond the scope of this paper and will be part of a follow-up paper (Mathur *et al.* 1993).

5. CONCLUSIONS

3C351 has been found to have a complex soft X-ray spectrum. Warm absorber, partial covering and soft excess models can all produce acceptable fits, although only the warm absorber model gives a good χ^2 for typical values for the high energy continuum slope.

Whichever model is correct this observation of 3C351 limits the possible causes for 'X-ray quietness'. Quasi-simultaneous X-ray, optical and ultraviolet (HST) observations of 3C351 make it highly unlikely that variability is the main cause of the wide range of α_{OX} observed in quasars. Spectral fits that allow for intervening absorption increase the intrinsic emitted X-ray flux of 3C351 by only a minor part of the difference in α_{OX} ($\approx$ 25%). If a warm absorber model applies then the α_{OX} of 3C351 originates not in an unusual X-ray spectrum but in a reduced normalization relative to the optical, indicating efficiency of X-ray production or a beamed component as the potential causes of different levels of X-ray emission. For the other models, extremely steep or extremely hard continua also contribute to the X-ray quietness of 3C351.

If a warm absorber model is assumed, then the strongest absorption edge feature lies in the range 0.58–0.76 keV (1σ, one interesting parameter), implying OIV–OVII as the most likely absorbing ions. The ionization parameter and column density of the absorber are constrained to $0.1 - 0.2$ and $1 - 5 \times 10^{22}$ atoms cm^{-2} respectively (for a power law ionizing continuum). Factor of two variability of the ionizing continuum should result in strong changes in the soft X-ray opacity of the warm absorber and so would provide a strong test for this model. Furthermore, observations of the source in different states of intensity would permit a constraint on the spectral index of the radiation incident on the absorbing gas (see the Appendix).

As noted in the Introduction, radio observations suggest that 3C351 is likely to be an almost edge-on quasar (e.g. Leahy and Perley 1991). Also, Eracleous and Halpern (1992) claim a double peaked $H\alpha$ emission line profile in this quasar. Double-peaked profiles are a signature of relativistic accretion disk viewed not face-on. This is consistent with the absence of any beamed component. Also, quite possibly our line of sight passes through gas at the edge of an "obscuring torus" suggested in Unified Models. 3C351 may provide a new tool for investigating conditions in this hypothesized torus, via variability monitoring or higher resolution spectra.

The PSPC energy band is particularly good to search for warm absorbers which reduce the 0.5-1 keV flux without totally removing photons in the 0.25 kev region, as can be seen from the color diagram in Figure 7 (see the Appendix). Since the region occupied by these warm absorber model in this diagram is well separated from the region occupied by simple power law plus cold absorption models (unless the column density is much lower than the Galactic one), such diagrams will be useful for selecting candidate warm absorbers. By using these diagrams it will be possible

to search efficiently for warm absorbers in large samples, for any source with at least 400 counts.

Acknowledgments

We would like to thank G. Ferland for providing us with the latest version of his photoionization code CLOUDY and A. Fazzolari and G.C. Perola for providing us with their compilation of atomic cross-sections and for many stimulating discussions. We thank also M. Birkinshaw for a careful reading of the manuscript and for his many comments. This work was supported by NASA grants NAGW-2201 (LTSARP), NAG5-1872 and NAG5-1536 (ROSAT), NASA contracts NAS8-39073 (AXAF Science Center), NAS5-30934 (Rosat Data Center), and NAS5-30751 (HEAO-2).

APPENDIX

The Behaviour of Warm Absorber Models

The behaviour of warm absorber models as α_E, U and N_H are changed is complex. This shows up clearly in the χ^2 contours in Fig. 5 which look quite different in ways that appear confusing. For $\alpha_E = 0.9$, U and N_H are strongly correlated and the gradients in the χ^2 surface on both sides of this correlation are very steep (for a given N_H the U is tightly constrained). For $\alpha_E = 0.7$ only the gradients going towards high N_H and low U are steep. For $\alpha_E = 0.6$ the gradients are rather shallow going towards both low and high U. For $\alpha_E = 0.5$ the gradients are again very steep going towards low U.

This apparently confusing situation can be understood more readily from Fig. 6 in which we show the transmitted spectra for $\alpha_E = 0.5$, 0.6, and 0.9, and for three values of U. It is instructive to compare the changes at 0.25 and 1 keV where the effects of Helium and Oxygen ionization, respectively, are dominant. For $\alpha_E = 0.9$ (and $N_H = 1.2 \times 10^{22}$), right panel, changing U through 0.12 and 0.18 produces a change in the opacity and so affects the transmitted spectrum mainly below 0.3 keV. The most prominent edge is that of O VII at 0.74 keV (except for U=0.18) and it is always deep enough to reproduce adequately the data around that energy. For $U \lesssim 0.14$ a large fraction of Helium and Carbon atoms are not completely ionized and give rise to a low energy cut-off too strong to be compatible with the data. For $\alpha_E = 0.6$, (and $N_H = 1.2 \times 10^{22}$), central panel, changing U through the same interval produces changes of comparable amplitude both at 0.25 keV and at 1 keV. The most prominent edge is that of O VII. For $\alpha_E = 0.5$, (and $N_H = 3.5 \times 10^{22}$), left panel, the changes at both 0.25 and 1 keV are very large. The most prominent edge is now that of O VIII at 0.87 keV. For $U \gtrsim 0.14$ most Helium and Carbon atoms are completely ionized as are a large fraction of Oxygen atoms and the O VIII edge is not deep enough to fit the data. When $U \lesssim 0.125$, Helium atoms are mostly neutral and contribute heavily to the absorption so the spectrum is strongly cut-off below ~ 0.3 keV.

The gradients in the χ^2 surfaces are steep going towards low U because the transmission at 0.25 keV saturates at unity as U increases well before the transmission at 1 keV, and since the χ^2 is more sensitive to the strength of the low energy cut-off than to the depth of the $\sim 0.7 - 0.9$ keV edge.

The amplitude of the changes at 1 keV increases going towards flatter α_E as Oxygen ionization grows rapidly. The amplitude of the changes at 0.25 keV decrease going from $\alpha_E = 0.9$ to $\alpha_E = 0.6$ and then increases again. For $\alpha_E = 0.6$ the $U - N_H$ allowed region is broader because while the O VII is always reasonably deep, the changes at 0.25 keV are smaller than for $\alpha_E = 0.7$ and 0.9.

Inspection of Figure 6 identifies two observationally convenient energy intervals, one centered around 0.25 keV and the other at 1 keV (in the quasar frame),

to which our modelling is particularly sensitive. They correspond, as noted above, to energies at which the opacity of Helium (and Carbon) and Oxygen, respectively, dominate. The level of agreement of a given model with the data is thus largely determined by the ratio between the flux at 0.25 and 1 keV. In Fig. 7 we plot the ratio between the expected PSPC counts in the intervals 1.2-2.4 keV and 0.6-1.0 keV as a function of the ratio between the counts in the intervals 0.2-0.4 keV and 0.6-1.0 keV (0.27-0.55 keV, 0.82-1.37 keV and 1.64-3.29 keV in the 3C351 frame) for three values of α_E and U in the range 0.1-0.2. The point with error bars represents the ratios actually measured in the case of 3C351 with the 1 σ uncertainty. The shape of the curves varies with α_E, while increasing N_H simply moves the $\alpha_E = 0.7$ curve towards lower values of the 0.2-0.4 keV/0.6-1.0 keV ratio and higher values of the 1.2-2.4 keV/0.6-1.0 keV ratio. This suggests that observations of the source in different states of intensity (and therefore with a different U) would permit a constraint on the spectral index of the radiation incident on the absorbing gas.

Color diagrams like that in Fig. 7 could also be a simple and useful tool to search for warm absorbers in AGN's in the PSPC energy band. In particular, absorbers in which most Helium atoms are completely ionized while Oxygen atoms are not, produce PSPC spectra significantly flatter in the keV region than at 0.25 keV. In a color-color diagram these models occupy a well defined region. As an example, the small stars in Fig. 7 represent the ratios computed from model 1 with absorption fixed at the Galactic value and α_E =2, 1.5, 1 and 0.5 (both ratios increase as the spectral index flattens). Increasing (decreasing) the N_H moves the points towards lower (higher) ratios. The big star represents the ratios computed from the best fitting model 1 (with $\alpha = 0.47$, $N_H = 3.9 \times 10^{19}$ cm^{-2}, much lower than the Galactic value along the line of sight): only for this extremely low value of the absorbing column does the point representing model 1 fall near some of the warm absorber models. It is however 6.2 σ and 3.7 σ from the corresponding ratios measured in the case of 3C351.

REFERENCES

Abramowitz M. and Stegun I. A. 1964, "Handbook of Mathematical Functions", National Bureau of Standards Applied Mathematical Series No. 55

Angione, R.J. 1973, AJ, 78 353

Avni, Y., & Tananbaum, H. 1986, ApJ, 305 83

Bahcall, J., *et al.* 1992, ApJ, submitted

Band, I.M., TrzhaskovsKaja, M.B., Verner, D.A., & Yakovlev, D.G. 1990, A&A, 237, 267

Barthel, P.D. 1989, ApJ, 336, 606

Blandford, R.D., & Kõnigl, A. 1979, ApJ, 232, 34

Cordova, F.A., Kartje, J.F., Thompson, R.J., Mason, K.O. Puchnarewicz, E.M., & Harnden F.R. 1992, ApJ, in press

Elvis, M., & Fabbiano, G. 1984, ApJ, 280, 91

Elvis, M., Lockman, F.J., & Wilkes, B.J. 1989, AJ, 97, 777

Elvis, M., Wilkes, B.J., & McDowell, J.C. 1991, "EUV Astronomy", eds R. Malina and S. Bowyer [New York: Pergamon], p. 238

Elvis, M., Giommi, P., Wilkes, B.J., & McDowell, J.C. 1991, ApJ, 378, 537

Elvis M. *et al.* 1993, in preparation.

Eracleous, M., & Halpern, J.P., 1992, "Testing the AGN Paradigm", eds. S.S. Holt, S.G. Neff and C.M. Urry AIP Conference Proceedings 254, p. 216

Fiore, F, Perola, G.C., Matsuoka, M., Yamauchi, M., & Piro, L. 1992, A&A., 262, 37

Ferland, G. 1991, "Hazy", OSU Astronomy Department Internal Report

Gioia, I.M., Maccacaro, T., Schild, R.E., Wolter, A., Stocke, J.T., Morris, S.L., & Henry, J.P. 1990, ApJS, 72, 567

Grandi, S., & Tifft W.G. 1974, PASP, 86, 873

Grevesse, N., & Anders, E. 1989, "Cosmic Abundances of Matter", AIP Conference Proceedings 183, ed. C.J. Waddington (New York: AIP).

Halpern, J.P. 1984, ApJ, 281, 90

Henke, B.L., Lee, P., Tanaka, T.J., Shimabukuro, R.L., & Fujikawa, B.K. 1982, Atomic Data and Nuclear Data Tables, 27, No. 1

Kellermann, K.I., Sramek, R., Schmidt, M., Shaffer, D.B., & Green, R. 1989, AJ, 98, 1195

Krolik, J.H., & Kallman, T.R., 1984, ApJ, 286, 366

Lampton, M., Margon, B., & Bowyer, S. 1976, ApJ, 208, 177

Leahy, J.P., & Perley, R.A. 1991, AJ, 102, 737

Orr, M.J.L., & Browne, I.W.A. 1982, MNRAS, 200, 1067

Makino, F., *et al.* 1989, ApJ(Lett.), 347, L9

Marscher, A.P. 1988, ApJ, 334, 552

Mathur, S., *et al.* 1993, in preparation

Morrison, R., & McCammon, D.A. 1983, ApJ, 270, 119

Nandra, K., Pounds, K.A., & Stewart, G.C. 1990, MNRAS, 242, 660

Nandra, K., & Pounds, K.A. 1992, Nature, 356, 215

Netzer, H. 1993, ApJ, in press
Pan, H.C., Stewart, G.C., & Pounds, K.A. 1990, MNRAS, 242, 177
Pfefferman, E., *et al.* 1987, Proc SPIE, 733, 519
Reilman, R.F., & Manson, S.T. 1979, ApJSuppl., 40, 815
Shastri, P., Wilkes, B.J., Elvis, M., & McDowell, J.C. 1993, ApJ, in press
Raymond, J.C., & Smith, B.W. 1977, ApJS, 35. 419
Tananbaum, H., Wardle, J.F.C., Zamorani, G., & Avni, Y. 1983, ApJ, 268, 60
Tananbaum, H., Avni, Y., Green, R.F., Schmidt, M., & Zamorani, G. 1986, ApJ, 305 57
Trümper, J. 1983, Adv. Space Res., 2, No. 4, 241
Turner, T.J., Weaver, K.A., Mushotzky, R.F., Holt, S.S., & Madejsky, G.M. 1991, ApJ, 381, 85
Turner, T.J., Done, C., Mushotzky, R., Madejski, G., & Kunieda, H. 1992, ApJ, 391, 102
Turner, T.J., & George, I. M. 1992, OGIP Calibration Memo
Veron-Cetty, M.-P., & Veron, P. 1991, ESO Scientific Report no. 10.
Wilkes, B.J., & Elvis, M. 1987, ApJ, 323, 243
Wilkes, B.J., *et al.* 1993, in preparation
Williams, O.R., *et al.* 1992, ApJ, 389, 157
Zamorani, G., *et al.* 1981, ApJ, 245, 357

Table 1: X-ray spectral fits to PSPC data for 3C351

model	$Norm.^a$	α_E	N_H^b	2nd Parameter	$\chi^2(dof)$
1 - power law	2.72 ± 0.17	0.47 ± 0.16	0.0039 ± 0.0027		61.1(28)
2 - 2 power laws	$2.79^{+0.38}_{-0.20}$	$-0.04^{+0.34}_{-0.25}$	0.048 ± 0.030	$\alpha_2 > 3.1$	26.8(26)
3 - partial covering	$13.9^{+4.4}_{-3.4}$	$2.12^{+0.42}_{-0.31}$	$2.00^{+0.69}_{-0.45}$	$F_C = 0.93^{+0.04}_{-0.05}$	26.2(27)
4 - power law +edge	5.06 ± 0.67	$0.96^{+0.15}_{-0.10}$	0.68 ± 0.09	$E_0^c = 0.68^{+0.10}_{-0.20}$	33.1(27)
5 - warm absorber	5.33 ± 0.70	0.5 FIXED	$3.90^{+0.25}_{-0.60}$	$U = 0.126^{+0.006}_{-0.002}$	28.8(28)
6 - warm absorber	$4.38^{+0.61}_{-0.50}$	0.6 FIXED	$1.35^{+0.75}_{-0.30}$	$U = 0.155^{+0.035}_{-0.025}$	28.9(28)
7 - warm absorber	$4.56^{+0.74}_{-0.64}$	0.7 FIXED	$1.17^{+0.48}_{-0.33}$	$U = 0.140^{+0.030}_{-0.020}$	30.0(28)
8 - warm absorber	5.22 ± 0.70	0.9 FIXED	1.30 ± 0.45	$U = 0.175 \pm 0.040$	31.4(28)
9 - warm absorber	5.41 ± 0.60	1.1 FIXED	1.20 ± 0.30	$U = 0.216 \pm 0.075$	32.8(28)

[a] at 1 keV, in units of 10^{-4} photons cm^{-2} s^{-1} keV^{-1}.
[b] in units of 10^{22} atoms cm^{-2}.
[c] in keV.

Table 2: 3C351, X-ray fluxes and luminosities

model	f_{PSPC} [a] (0.1-2.45 keV)	f_{IPC} [a] (0.5-4.5 keV)	L^b (0.1-2.45) keV	α_{OX}
1 - power law	$1.08^{+0.13}_{-0.10}$	$1.25^{+0.15}_{-0.12}$	$1.11^{+0.10}_{-0.08}$	1.59
2 - 2 power laws	> 2.4	> 2.3	> 1.3	1.52
3 - partial covering	25^{+41}_{-13}	$3.9^{+1.4}_{-0.9}$	16^{+19}_{-7}	1.60
8 - warm absorber ($\alpha_E = 0.9$)	2.5 ± 0.4	1.5 ± 0.3	2.0 ± 0.5	1.54

[a] unabsorbed flux in units of 10^{-12} erg cm^{-2} s^{-1};
[b] in units of 10^{45} erg s^{-1}
(assuming $H_0 = 50$ km s^{-1} Mpc^{-1} and $q_o = 0$, z=0.37)

FIGURE CAPTIONS

Figure 1. Single power law with low energy "cold" absorption spectral fit to the spectrum of PG1426+015. Energies are in the observed frame.

Figure 2. Single power law with low energy "cold" absorption spectral fit to the spectrum of 3C351. Energies are in the observed frame.

Figure 3. Residuals of fit to the spectrum of 3C351 for (a) two power laws model (soft component), (b) Partial covering model, (c) single power law plus absorption edge. Energies are in the observed frame.

Figure 4. (a) Warm absorber model spectral fit to the spectrum of 3C351 (α_E fixed at 0.9). (b) The best fitting transmitted spectrum. The deep edge at $\sim$ 0.74 keV is due to Oxygen VII. Energies are in the quasar frame.

Figure 5. The $U - N_H$ 68 %, 90 % and 99 % confidence contours for the warm absorber model for $\alpha_E = 0.5$, 0.6, 0.7 and 0.9.

Figure 6. The transmitted spectra for $\alpha_E = 0.5$, $N_H = 3.5 \times 10^{22}$ cm^{-2}, left panel (A), $\alpha_E = 0.6$, $N_H = 1.2 \times 10^{22}$ cm^{-2}, central panel (B), and $\alpha_E = 0.9$, $N_H = 1.2 \times 10^{22}$ cm^{-2}, right panel (C), and for five values of the ionization parameter.

Figure 7. The ratio between the counts in the energy intervals 1.2-2.4 keV and 0.6-1.0 keV plotted as a function of the ratio in the intervals 0.2-0.4 keV and 0.6-0.9 keV for α_E=0.5, $N_H = 1.2 \times 10^{22}$ cm^{-2} (crosses), α_E=0.7, $N_H = 1.2 \times 10^{22}$ cm^{-2} (filled squares), α_E=0.7, $N_H = 1.5 \times 10^{22}$ cm^{-2} (open squares), and α_E=0.9, $N_H = 1.2 \times 10^{22}$ cm^{-2} (open circles). In all cases U is varied between 0.1 and 0.2. The point with error bars represents the ratios measured from the 3C351 spectrum with the 1 σ uncertainty (no systematic error has been added here to the statistical error in each channel). The big star represents the ratios computed from the best fitting model 1 in Table 1. The small stars represent the ratios computed from model 1 with absorption fixed at the Galactic value of 2.26×10^{20} cm^{-2} and α_E =2, 1.5, 1 and 0.5 (both ratios increase as the spectral index flattens). Increasing (decreasing) the N_H moves the points towards lower (higher) ratios.

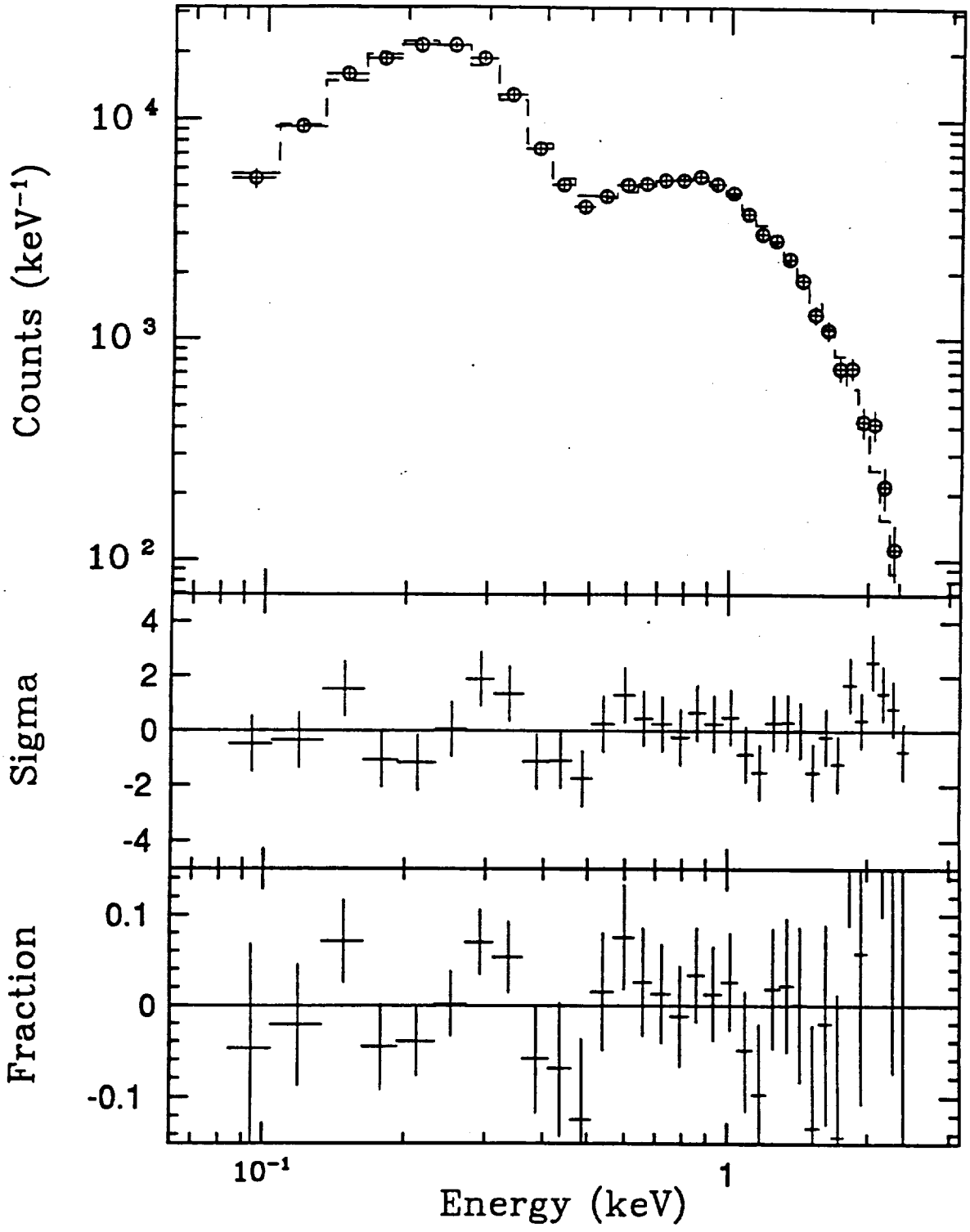
Counts (keV⁻¹)
10⁴
10³
10²
Sigma
4
2
0
-2
-4
Fraction
0.1
0
-0.1
10⁻¹
1
Energy (keV)

Fig. 1

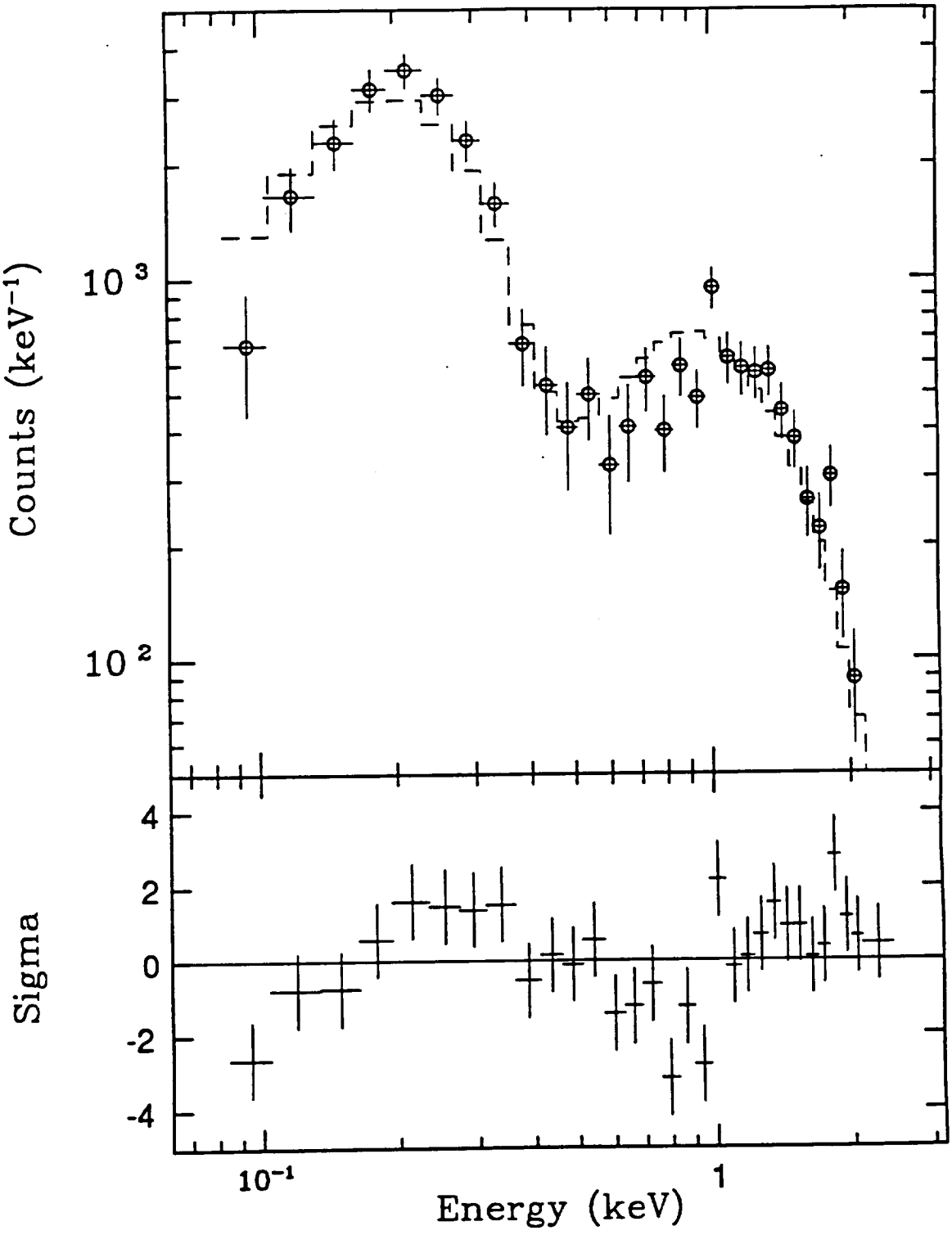

Fig. 2

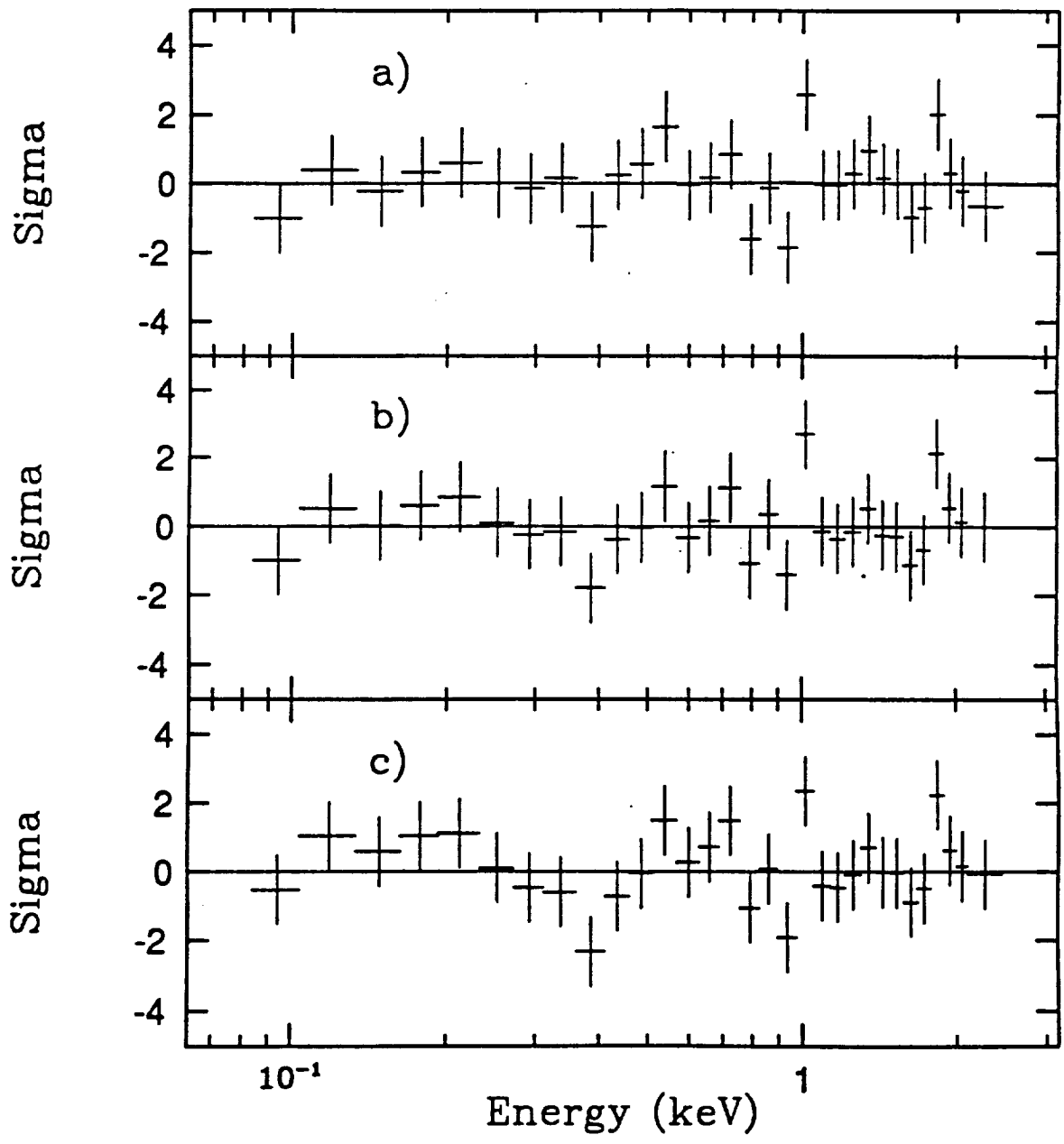

Fig. 3

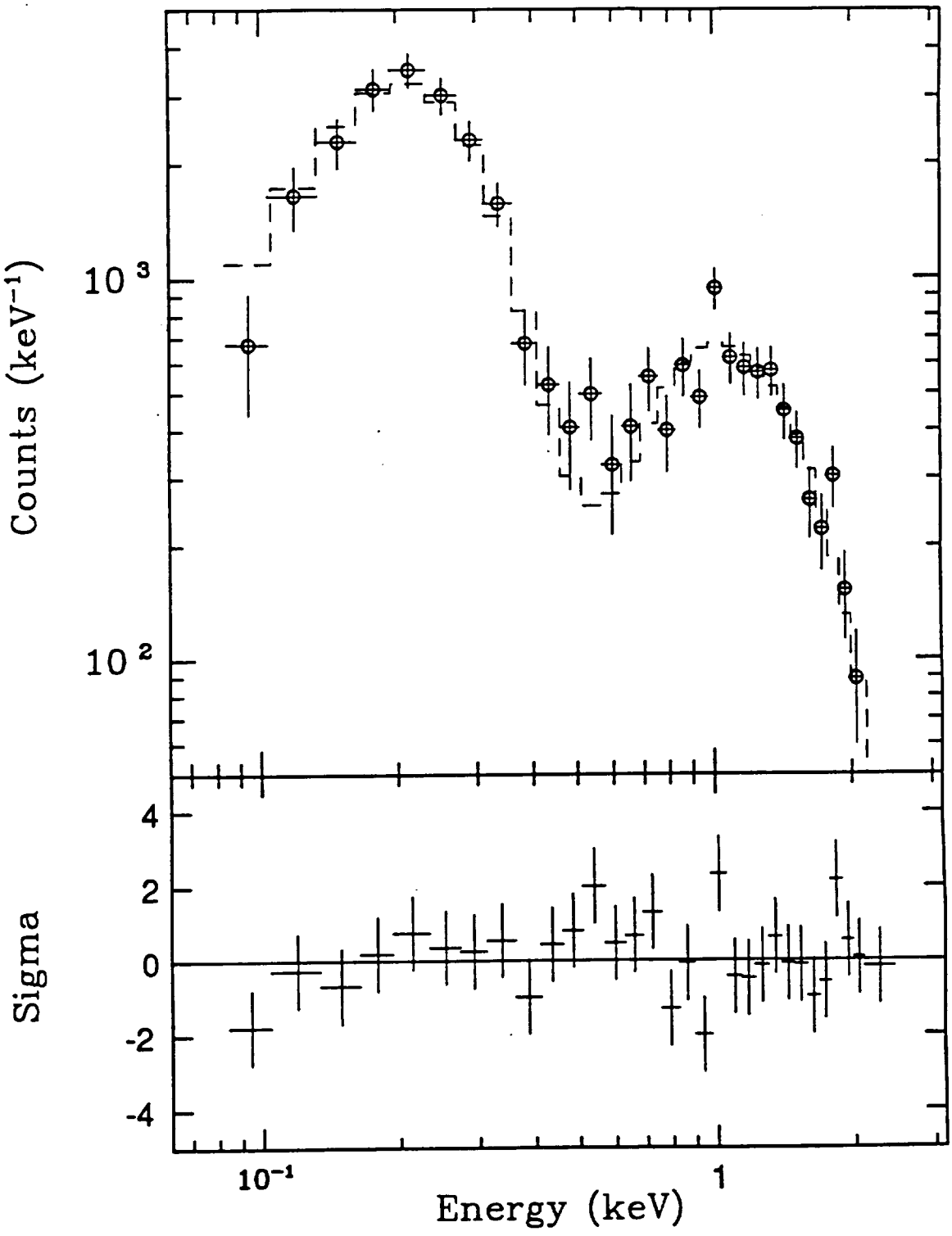

Fig. 9e

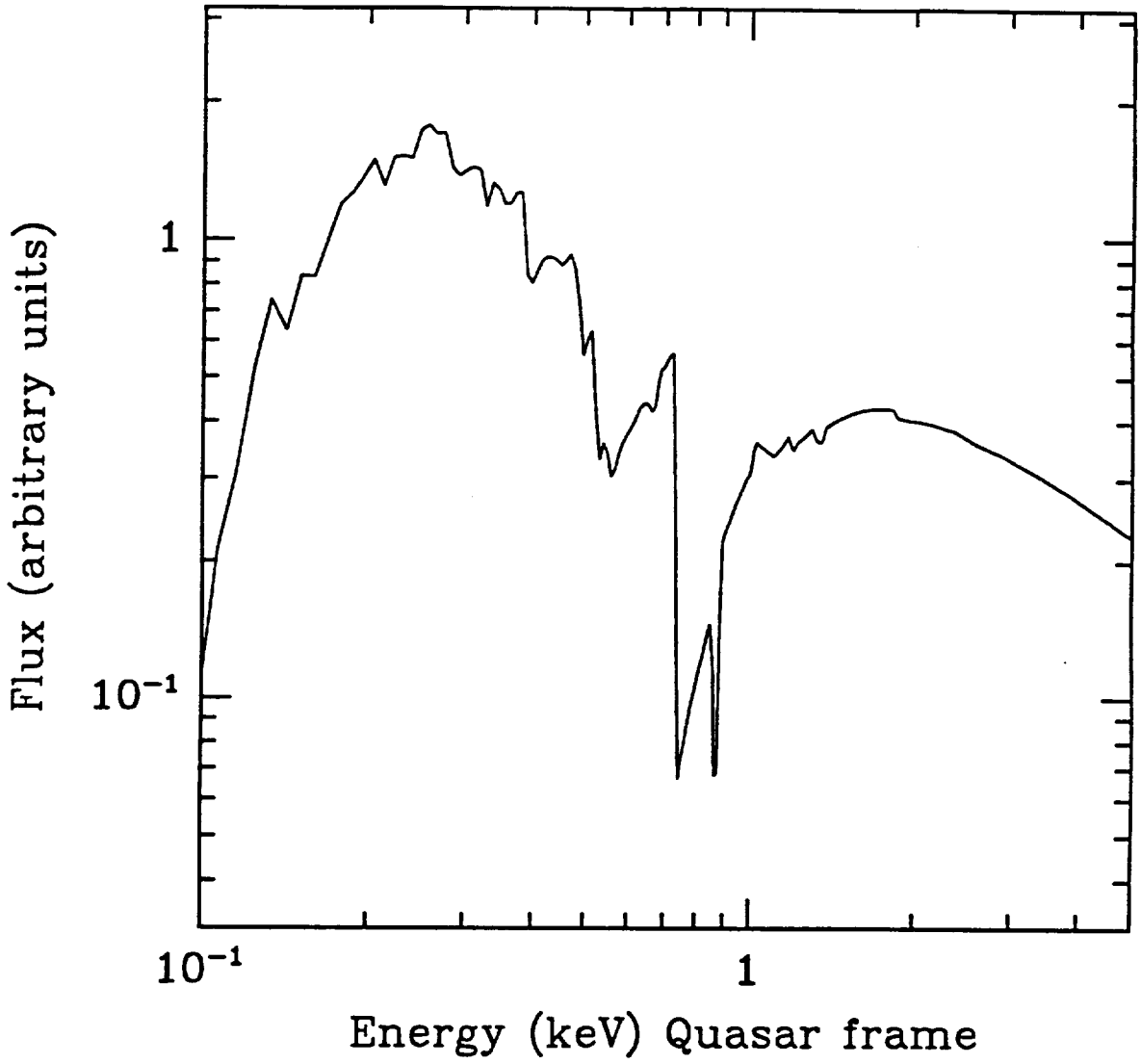

Fig. 46

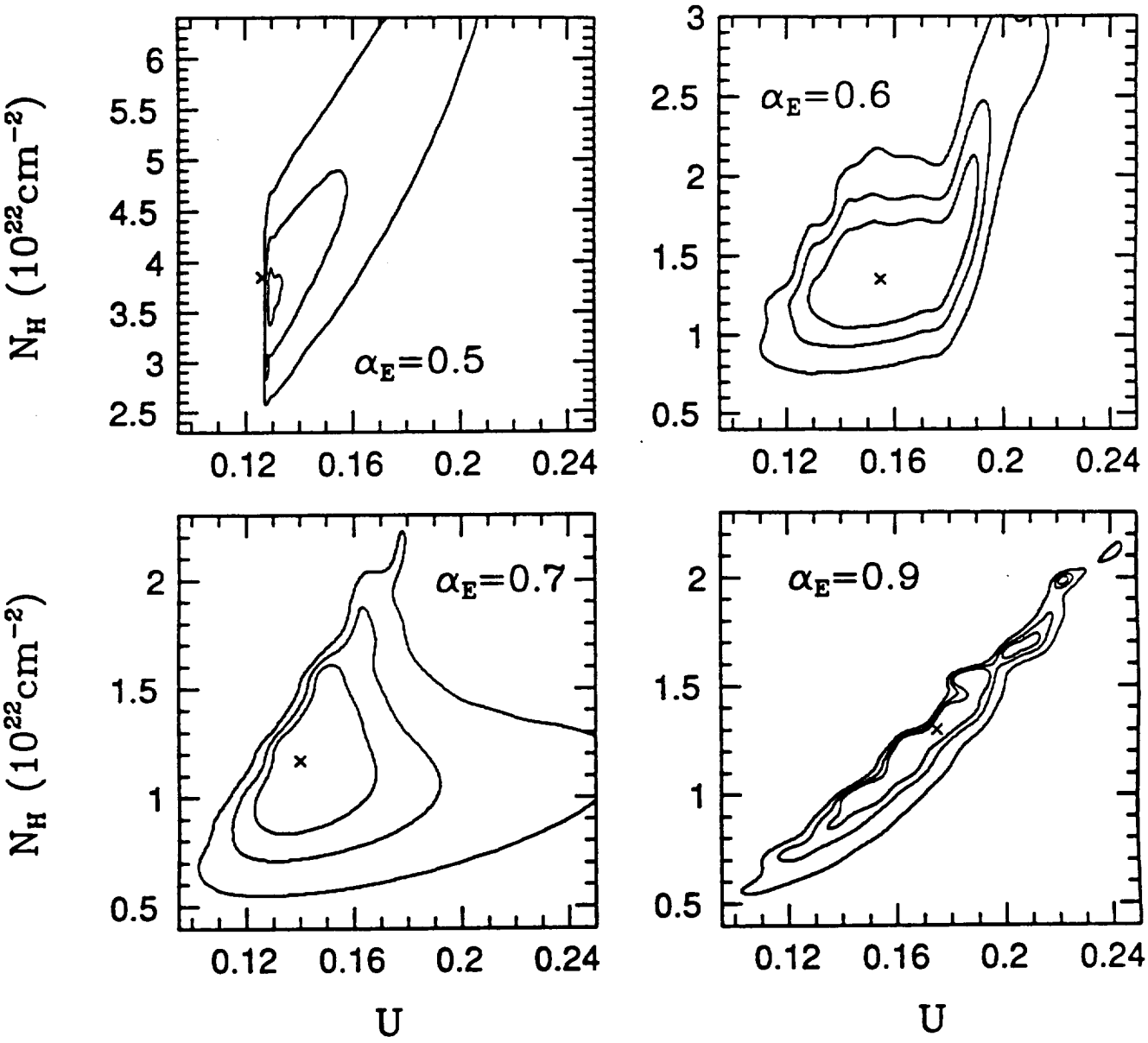
N_H (10^{22}cm^{-2})
α_E=0.5
α_E=0.6
α_E=0.7
α_E=0.9
U
0.12
0.16
0.2
0.24

Fig. 5

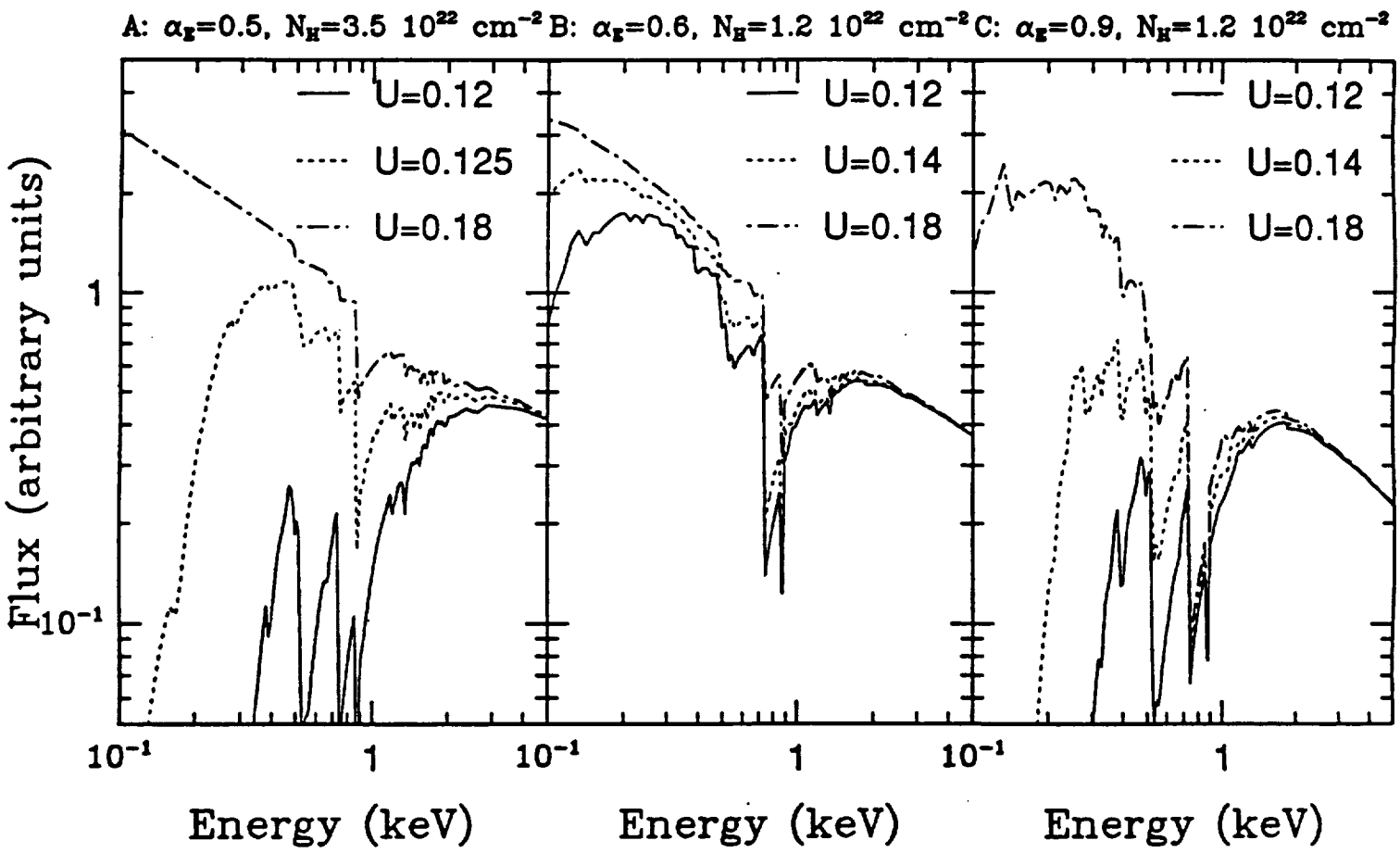
A: α_E=0.5, N_H=3.5 10^{22} cm^{-2} B: α_E=0.6, N_H=1.2 10^{22} cm^{-2} C: α_E=0.9, N_H=1.2 10^{22} cm^{-2}
U=0.12
U=0.125
U=0.18
U=0.12
U=0.14
U=0.18
U=0.12
U=0.14
U=0.18
Flux (arbitrary units)
1
10^{-1}
10^{-1}
1
10^{-1}
1
10^{-1}
1
Energy (keV)
Energy (keV)
Energy (keV)

Fig. 6

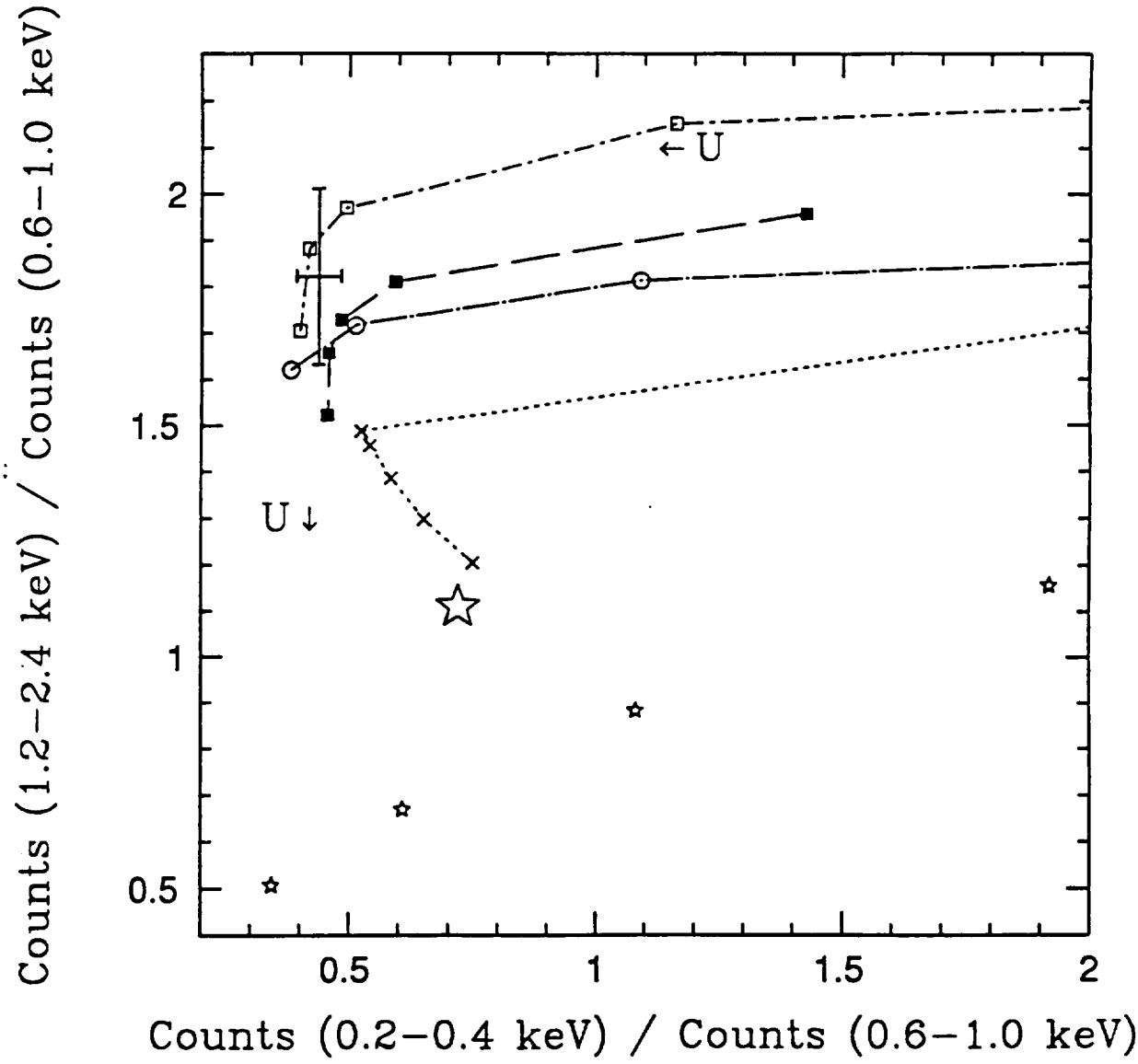
Counts (1.2–2.4 keV) / Counts (0.6–1.0 keV)
Counts (0.2–0.4 keV) / Counts (0.6–1.0 keV)
0.5
1
1.5
2
0.5
1
1.5
2
← U
U ↓

Fig. 7

ABSORPTION IN X-RAY SPECTRA OF HIGH REDSHIFT QUASARS

Martin Elvis, Fabrizio Fiore, Belinda Wilkes, Jonathan McDowell
Harvard-Smithsonian Center for Astrophysics
60 Garden St, Cambridge MA 02138

and

Jill Bechtold
Steward Observatory, University of Arizona
Tucson AZ 85721

Accepted for publication in The Astrophysical Journal
12 July 1993

Abstract

We present evidence that X-ray absorption is common in high redshift quasars. We have studied six high redshift (z$\sim$3) quasars with the ROSAT PSPC of which four are in directions of low Galactic N_H. Three out of these four show excess absorption, while only three in about fifty $z \lesssim 0.4$ quasars do, indicating that such absorption must be common, but not ubiquitous, at high redshifts, and that the absorbers must lie at z>0.4.

The six quasars were: S5 0014+81, Q0420−388, PKS0438−436, S4 0636+680, PKS2000−330, PKS2126−158, which have redshifts between 2.85 and 3.78. PKS0438−436 and PKS2126−158 show evidence for absorption above the local Galactic value at better than 99.999% confidence level. If the absorber is at the redshift of the quasar then values of $N_H=(0.86^{+0.49}_{-0.28}) \times 10^{22}$ atoms $cm^{-2}$for PKS0438−436, and $N_H=(1.45^{+1.20}_{-0.64}) \times 10^{22}$ atoms cm^{-2} for PKS2126−158, are implied, assuming solar abundances. The spectrum of S4 0636+680 also suggests the presence of a similarly large absorption column density at the 98% confidence level.

This absorption reverses the trend for the most luminous AGN to have the least X-ray absorption, so a new mechanism is likely to be responsible. Intervening absorption due to damped Lyman-α systems is a plausible cause. We also suggest, as an intrinsic model, that intracluster material, *e.g.* a cooling flow, around the quasar could account for both the X-ray spectrum and other properties of these quasars. All the quasars are radio-loud and three are Gigahertz Peaked (2 of the 3 showing absorption).

No excess absorption above the Galactic value is seen toward Q0420−388. This quasar has two damped Lyman-α systems at z=3.08. The limit on the X-ray column density implies a low ionization fraction, $N(HI)/N(H) \gtrsim 4 \times 10^{-3}$ (3σ), for solar abundances, for these systems, and can set a weak limit on the size of the absorber.

In the emitted frame these PSPC spectra cover the band $\sim$0.5-10 keV, which has been well observed for low redshift quasars and AGN. Comparison of high and low redshift spectra in this emitted band show no change of mean spectral index greater than $\Delta\alpha_E > 0.3$ (99% confidence) with either redshift or luminosity, for radio-loud quasars.

1. INTRODUCTION

The strong evolution shown by quasars with redshift must be fundamental in understanding what these objects are and how they form. By z=3 a typical quasar [1] is 50-100 times more luminous than a local one (Boyle *et al.* 1987, 1993). The quasar continuum spans all wavelengths, yet quasars at redshifts above one have so far been studied in detail only in the optical and radio bands. In particular, the X-ray emission from quasars carries a significant fraction of their bolometric luminosity (*e.g.* Elvis *et al.* 1993). Since X-rays are likely to come from the immediate neighborhood of the "central engine" the X-ray properties of high redshift quasars will surely provide clues to understanding quasar evolution. X-ray spectra also provide a new means of studying the intervening systems along the line of sight to high redshift quasars through photoelectric absorption appearing at low energies.

ROSAT is a good instrument for these studies because of its high sensitivity. Moreover the rest energy range observed by ROSAT at z=3 is ~0.5-10 keV, which is similar to the range in which most of the low redshift quasars have been observed with the EXOSAT and *Ginga* satellites. This makes it possible to search for evolutionary changes in the same emitted energy band by comparing ROSAT spectra of high redshift quasars with already measured spectra of objects at low redshift.

We have initiated a program to study high z quasars with the ROSAT PSPC. Wilkes *et al.* (1992) reported a first detection of excess absorption toward a high z quasar. We now have observations of six quasars with redshifts ranging from 2.85 to 3.78, and we find two more cases of likely strong absorption in their X-ray spectra.

In this paper we present spectra for the four quasars at $z \gtrsim 3$ for which we have more than 350 counts, and simple X-ray colors for two $z > 3$ quasars which have ~60 counts. A separate paper will discuss the X-ray fluxes and overall spectral energy distributions of all the quasars for which we have detections (Bechtold *et al.* 1993, in preparation). Observational feasibility constrained our selection of objects to those with either known high X-ray fluxes or bright apparent optical magnitudes. Combined with the requirement of high redshift, this biases our quasar sample toward the most luminous objects in the universe.

We assume a Friedmann cosmology with $H_0 = 50$ km s^{-1} Mpc^{-1} and $\Omega_0 = 0$.

2. OBSERVATIONS

ROSAT (Trümper 1983) observed the high redshift quasars reported here with the Position Sensitive Proportional Counter (PSPC, Pfefferman *et al.* 1987) between February 1991 and September 1992. Details are given in Table 1. Each of the quasars was detected as an X-ray source, and the PSPC derived position for the

[1] *i.e.* one at L*, the luminosity at which the luminosity function changes slope.

quasars lie within 12 arcseconds of the accurate optical positions of Schneider *et al.* (1992) with exception of the February 1991 observation of PKS0438−436. The PSPC position in the Standard Analysis Software System (SASS) processing for the X-ray source identified with PKS0438−436 in this observation is 2.9′ from the quasar optical position. However we are confident of the identification because a second quasar in the field, PKS0439−433 is also offset in the same direction by 2.6′. The difference in offsets of 18″ is similar to the PSPC beamsize. PKS0439−433 is well off-axis and close to a support structure which may induce an additional slight offset. Aspect errors of this size have been seen in a few other ROSAT pointings with the current version of the SASS (ROSAT Newsletter no.10, 1992). Also the second observation in 1992 September gives a position for PKS0438−436 within six arcseconds of the optical position.

For six of the observations the standard 'wobble' mode was on (Table 1). In this mode the detector is moved to and fro along a 3 arcmin path with a 400 second period, to smooth out detector structure. In the other two observations the wobble was turned off. The source counts reported in Table 1 are net counts within a circle of radius 2 arcminutes around the X-ray centroid of the source, enclosing 95% of the counts in a point source (Turner and George 1992). For the wobbled observations and for the observation of Q0420−388 the background spectra were taken from an annulus of inner and outer radii 2.5 arcmin and 5 arcmin. Background subtraction for the unwobbled observation of PKS0438−436 is described below. The source counts do not increase significantly considering broader source and background regions both in the 0.1-2.5 keV and the 0.1-0.3 keV energy bands, suggesting that any "electronic ghost images" that form at low energies, below ∼0.15 keV (Turner and George 1992), are unimportant in these observations. The 34 energy channels from the MPE SASS pipeline processing were used in this analysis.

The pulse height (PHA) spectra are shown in figure 1 for the four quasars with more than 350 counts. Three of these show a marked absence of low energy counts. Such low energy cut-offs are a characteristic signature of photoelectric absorption. To quantify this impression fits of simple power laws with the flux reduced at low energies by photoelectric absorption due to cold material at cosmic abundances (cross sections from Morrison and McCammon, 1983) were made (Table 2, fit 1). In Table 2 we give the values of the fitted parameters, the normalization, the energy spectral index α_E and the column density N_H (the errors represent the 68 % confidence intervals for two interesting parameters when both α_E and N_H are free to vary, and for a single interesting parameter when N_H is fixed). We also list in Table 2 the reduced χ^2 for the fit and the number of degrees of freedom (dof). The January 1993 version of the PSPC response matrix (DRM_36_1) was used in this analysis. The fit parameters do not differ significantly from those obtained with the March 1992 matrix (DRM_9), suggesting that calibration systematic uncertainties are small and negligible in comparison to the statistical uncertainties. In the analysis we included,

however, a systematic error of 1%, as suggested by Hasinger and Snowden 1992. The fits were performed over the 0.1-2.45 keV energy range (channels 3-34).

In all cases the χ^2 values are consistent with the simple power law plus absorption model (fit 1), which is unsurprising given the limited number of counts in the spectra. For two of the quasars though, the allowed values of N_H are larger than the Galactic value. Fits with N_H fixed at the Galactic value (fit 2) do not give acceptable fits for these quasars. Figure 2 shows 68 %, 90% and 99% confidence contours in ($log N_H$, α) space (solid lines). These do not overlap the Galactic value of N_H for PKS0438−436 or PKS2126−158. Fits with an additional absorber at the redshift of the quasars (fit 3) suggests large column densities (figure 1 fits and residuals, figure 2 - thicker lines).

The X-ray absorption cut-off, although conventionally reported as a hydrogen column density, in fact measures the total column density toward the object, not just the neutral hydrogen column. Around a kilovolt, where the cut-offs in the X-ray spectra of PKS2126−158 and PKS0438−436 are seen (in the quasar frame) the X-ray absorption cross-sections for metals (primarily the K-edges of Oxygen, and to a lesser extent to C, Ne, Mg, Si, S and Fe) are 5-10 times larger than the H+He cross-sections (Morrison and McCammon 1983). The metals can be in small dust grains and still produce X-ray absorption (until the grains grow big enough to shield their inner parts), with only minor modifications to their cross-sections (Fireman 1974). Only fully ionized material has no effect. Since metal abundances at high redshift could well be 1/10 solar or less (Meyer and Roth 1990, Pettini, Boksenberg and Hunstead 1990, Turnshek *et al.* 1989) we have also made power-law spectral fits with an absorber of varying abundance at the quasar redshift. For a sake of simplicity the relative abundances among different metals have been fixed at the Morrison and McCammon (1983) values. We therefore increased the number of degrees of freedom only by one, the ratio R between the metal abundances (C, N, O, Ne, Mg, Si, S, Ar, Ca and Fe) at the quasar redshift to the solar ones. The fits to the coadded spectra of PKS0438−436 and PKS2126−158 (see Sections 2.3 and 2.4) give the same χ^2, and spectral indices (to within $\pm$ 0.05) for a range of R from 0 to 2. The PSPC cannot distinguish the shape of solar and zero metal abundance absorption in these high z quasars. As would be expected R is strongly anticorrelated with N_H, as is shown in figure 3, where we plot the best fit values of the two parameters for both quasars. When assuming only the H+He cross-sections appropriate to primordial material (R=0) the N_H required to fit the data adequately is about four times that obtained when R=1 (while $N_H(R = 0.1) \sim 3N_H(R = 1)$). At higher R the N_H values decrease inversely with R.

The PSPC does not constrain the redshift of the absorbing material. The derived column density increases as $z_{absorber}$ is increased, since the absorbed photons gain energy as (1+z). Figure 4 shows the constraints on the N_H of the absorbing material as a function of its assumed redshift for the two quasars with strong N_H.

A power-law with photoelectric absorption is not the only possible model that can give low energy cut-offs. We also fitted black body models to the PSPC spectra. These fits gave best fit temperatures of 0.9−1.6 keV, so that the low energy cut-off is modelled as the Rayleigh-Jeans tail. In all four cases however, the χ^2 values were worse than for the power-laws, and were rejectable at the 95% level or higher. Given the limited energy resolution of proportional counters, strong Fe-L line emission from an optically thin plasma at around 1 keV (Raymond and Smith 1977) can simulate a power-law with a low energy cut-off. However, at z=3, this emission is redshifted to $\sim \frac{1}{4}$ keV where it would produce a soft excess rather than a deficit. The ~4 keV region that is redshifted into the 1 keV band is relatively free of strong emission line features. Fits to Raymond plasmas gave acceptable χ^2 values (for 50% solar abundances, with redshifts fixed at the quasar value), but only for temperatures above the range that can be well determined by ROSAT at this signal-to-noise (kT=4−13 keV), as well as excess column densities. Such high temperatures have little line emission so that in the PSPC range they are essentially power laws. Since power-law fits are better constrained we did not consider optically thin thermal models further. It should be noted that no simple model need be appropriate. Complex X-ray spectra in AGN are becoming required as signal-to-noise and resolution improve (e.g. Fiore et al., 1993, Marshall et al. 1993). While better measurements are needed, we shall adopt the straightforward absorbed power-law model in the remainder of this paper.

The observed energy of the iron K fluorescence line (6.4 keV rest frame) is within the ROSAT band for z>2. ROSAT observations of high redshift quasars can therefore constrain the amount of K-fluorescence emission in these quasars, albeit weakly. We fitted a power law plus absorption model (model 3) adding a narrow gaussian line at the fixed, redshifted, energy of the 6.4 keV Fe-K fluorescence line to the PSPC spectra. These limits on rest equivalent width are also given in Table 2 and lie in the range 0.7-1.5 keV (90% confidence).

Table 3 gives fluxes and luminosities derived from the single power-law fits for each quasar. Systematic errors for the wobbled observations are ~4% (Schlegel E., priv. comm.). Uncertainties in the luminosities quoted are dominated by the choice of cosmological parameters. The luminosities in table 3 are reduced by factors of about four for Ω_0=1, depending on each object's redshift. For reference 3C273 has a luminosity of 1×10^{46} erg s^{-1} (2-10 keV, Williams *et al.* 1992), 1% - 10% of the luminosity of these quasars.

Below we give some details on each of the quasars.

2.1 S5 0014+813, z=3.38

This radio-loud quasar is bright in X-rays, with an observed 0.1-2.5 keV flux of about 2×10^{-12} erg cm^{-2} s^{-1}. It is the only z>3 quasar to have a previously reported X-ray spectrum (Lawson *et al.* 1992), obtained with EXOSAT.

The best fit value of the column density N_H is consistent with the rather

large Galactic value of 1.4×10^{21} cm^{-2}, as the lack of low energy counts in figure 1a suggests. If the N_H is fixed to the Galactic value then the spectral index obtained is $\alpha_E = 0.82 \pm 0.19$ (1 σ error for one interesting parameter).

This quasar was observed with EXOSAT in 1984 November. The spectral index reported by Lawson et al. (1992) is 0.9 ± 0.4 (1 σ error for one interesting parameter), thus suggesting that the 4−40 keV (rest frame) spectrum does not present large departures from the power law slope found by ROSAT. S5 0014+813 was not observed with the *Einstein* IPC, since it had not been discovered when *Einstein* was functioning.

2.2 Q0420−388, z=3.12

This is the only optically selected (Osmer and Smith 1977) quasar in our sample with sufficient counts to obtain a good spectrum (shown in figure 1b). It is not however radio-quiet. In fact Q0420−388 is quite a strong radio source (Condon *et al.* 1981). Radio-loudness is normally evaluated between the optical B band and 5GHz, $R_L = log(f_{(5GHz)}/f_B)$, with radio-loud objects having $R_L > 1$. Q0420−388 has $R_L = 2.24$ (using Condon *et al.* 1981 for the 1.4GHz radio flux and Hyland and Allen 1982 for the H magnitude, which lie closest to the emitted fiducial frequencies), and so is radio-loud. Q0420−388 is also a candidate Gigahertz Peaked Spectrum source (GPS, O'Dea 1990), with a cut-off at ∼1.5 GHz (observed frame, Condon *et al.* 1981).

There were problems in two of the eight observing intervals ("OBI") of this observation, due to mispointing of the satellite. For the present analysis we used only the first four and the last two observing intervals, giving a total integration time of 11896 sec. Although the wobble was off for this observation the standard source and background regions were used since the problems encountered for PKS0438−436 (see below) were not present. The results are stable if the background region is moved by small amounts.

The large number of low energy counts suggests little absorption and the best fit value of N_H is consistent with the low Galactic value of 1.9×10^{20} atoms cm^{-2}(figure 2). The spectral index obtained by fixing N_H to the Galactic value is $\alpha_E = 0.73 \pm 0.10$, consistent with the mean value found in radio-loud low redshift quasars in the 1−10 keV rest frame band (Williams et al. 1992, Lawson et al. 1992), and in the 0.2-3.4 keV band (Wilkes and Elvis 1987, Shastri *et al.* 1993).

The PSPC count rate of 0.031 ct s^{-1} is about double the 1979 *Einstein* IPC count rate of 0.016 ct s^{-1} (Harris *et al.* 1990). Given the relative sensitivity of the telescopes this is consistent with no flux variations between the two observations (ROSAT Mission Description 1991), assuming the best fit PSPC spectrum.

2.3 PKS0438−436, z=2.85

We now have double the exposure time on this quasar compared with that reported by Wilkes *et al.* (1992), thanks to a second observation 18 months after

the first (Table 1). We first repeated the analysis of the 1991 February observation following Wilkes *et al.* (1992) but using a larger region to collect the lowest energy counts. (The 'electronic ghost images' problem was only widely known after that paper was completed.) This results in 7% more counts and a better fit at low energies. The effect of the wobble being off in this observation is that an estimate of the background from our standard annulus around the source gives negative counts in the first 6 channels. This is because the background just around source is lower than average (probably due to shadowing by the wires supporting the window), while our standard background annulus captures a higher, and inappropriate, background. The best background subtraction (the one which minimizes the problem in the first channels) is obtained by taking the background along the shadow of the wires in a rectangular region to the south of the source. Adding these low energy counts does not remove the absorption reported by Wilkes *et al.* (1992). The power law slope is better constrained on the steep side in our new fit (Table 2). During the second, 1992 September, observation the wobble was on and the background subtraction was performed as described at the beginning of this section.

The 1991 February and 1992 September pulse height spectra were very similar, as were the best fit parameters (Table 2) with exception of the normalization, which is 40% lower in the second observation (a 1.8σ difference). Due to the lack of spacecraft wobble, the flux measured during the earlier observation is a lower limit to the real source flux, as the fraction of the observation for which the source may have been occulted by the support wires is uncertain. The real source flux could be as high as twice the value reported in Table 3. It is therefore possible, but not required, that the source faded by 20%–50% in the 1.58 years (0.41 years in the quasar frame) between the two observations. The 1992 September flux is consistent with the $(4.8\pm0.40)\times10^{-13} erg\ cm^{-2}\ s^{-1}$ measured by the *Einstein* IPC in 1979 March (0.16–3.5 keV, α_E=0.5, Wilkes *et al.* 1993). Since the shapes of the two spectra are similar, in spite of possible flux variations, we combined the two spectra to improve to signal to noise ratio.

The best fit value of the absorbing column in the coadded spectrum ($N_H = (6.9^{+3.5}_{-1.8}) \times 10^{20}$ cm $^{-2}$, 1σ error for two interesting parameters, α_E and N_H), is not consistent with the Galactic value at a high confidence level (>99.9999 % ,$\Delta\chi^2$ = 45.2, for one additional degree of freedom). A spectral fit with local absorption fixed at the Galactic value plus free absorption at z=2.85 yields an intrinsic N_H of $(0.86^{+0.49}_{-0.28}) \times 10^{22}$ cm^{-2} and a slope $\alpha_E = 0.61 \pm 0.22$.

2.4 PKS2126−158, z=3.27

This is another radio-loud quasar with a Gigahertz peaked spectrum (O'Dea, Baum and Stanghellini 1991), with a clear break at ~5 GHz (observed frame, Peterson *et al.* 1982). It is bright in X-rays, with a PSPC flux of 3.7×10^{-12} erg cm^{-2} s^{-1} (0.1-2.5 keV). We observed the source twice, in May 1991 and November 1992, obtaining a

similar count rate. The PSPC count rate of 0.17 ct s^{-1} is 1.9 times the 1979 *Einstein* IPC count rate of 0.09 ct s^{-1} (Worrall and Wilkes, 1990), consistent with no variation between the two observations (see §2.2, ROSAT Mission Description 1991). (Also the HST snapshot survey found that PKS2126−158 had V=17.2±0.2 on 1991 June 6 (Maoz *et al.* 1992), only one month after our ROSAT observation and consistent with the V=17.3 Palomar Sky Survey magnitude, Jauncey *et al.* 1978).)

The two PSPC spectra were very similar, as were the best fit parameters in Table 2, and therefore we combined the two spectra together to improve the signal to noise ratio. The coadded spectrum is shown in figure 1d where a deficit of low energy counts can be seen similar to that in S5 0014+81 and PKS0438−386. The Galactic N_H toward PKS2126−158 is only 4.85×10^{20} atoms cm^{-2}, so that excess absorption is again suggested. Indeed, while the spectral index is consistent with the mean spectral index found in low redshift radio loud quasars, the best fit value of the absorbing column ($N_H = (12.9^{+7.2}_{-3.8}) \times 10^{20}$ cm $^{-2}$, 1σ error for two interesting parameters, fit 1), is not consistent with the Galactic value at high confidence level (> 99.999 %, $\Delta\chi^2 = 28.9$, for one additional degree of freedom, fit 2). N_H is significantly greater than the Galactic value in both observations (at the 99% and 99.99% confidence level, respectively).No other bright source is present in the PSPC image so that, unlike the case of PKS0438−386 (Wilkes *et al.* 1992), we do not have an independent test against transient instrumental or local Galactic N_H peculiarities.

A spectral fit with local absorption fixed at the Galactic value plus free absorption at z=3.27 (fit 3) yields an intrinsic N_H of $(1.45^{+1.20}_{-0.64}) \times 10^{22}$ cm^{-2} while not changing significantly the slope ($\alpha_E = 0.52^{+0.25}_{-0.21}$). Worrall and Wilkes (1990) also found evidence for absorption in excess of the Galactic value in PKS2126−158 at the 98.79% confidence level, implying that the absorption we see is not transient.

2.5 S4 0636+680 (z=3.18), PKS2000−330 (z=3.78)

For the two quasars with ∼60 counts we investigated the possibility that they might also have additional absorbing column density. We did this by fixing the spectral index in the fit to the mean of the other four, and allowed the intrinsic absorbing column density to vary. The resulting fits are given in table 2.

With this prescription S4 0636+680 shows evidence for additional absorption beyond the Galactic value (at 98% confidence, $\Delta\chi^2 = 5.6$, for one additional degree of freedom), at a level similar to that of PKS2126−158 and PKS0438−436. Only for power law slopes flatter than α_E= 0.2 (68 % confidence) does the spectrum of S4 0636+680 become consistent with the Galactic column density. Such a flat slope would be rare. Of 13 quasars studied in this energy range by *Ginga*, Williams *et al.* (1993) found only one, PG1416-129 with a slope this flat (α_E=$0.10^{+0.16}_{-0.21}$), and the next flattest had α_E >0.4. On average flat spectrum radio core dominated quasars have flat slopes (Shastri *et al.* 1993) but these too are predominantly steeper than α_E >0.4. In contrast S4 0636+680 has a steep high frequency radio spectrum (Kuhr

*et al.*1981, and is a strong GPS candidate (O'Dea *et al.* 1991).

The X-ray spectrum of PKS2000−330 is consistent with the Galactic absorption, but the rather large value of the Galactic column density, and the limited number of counts prevent the detection in this spectrum of an additional column density similar to that detected in the other quasars. PKS2000−330 is also a candidate GPS source in the list of O'Dea *et al.* (1991).

3. DISCUSSION

The ROSAT results reported here extend the study of quasar spectra to double the previous logarithmic range of luminosity, and increase the range of redshift from about 0.3 to three. Although we have so far only four objects with determined spectra, we can set interesting limits on any change in mean X-ray slope with luminosity or redshift.

The major, and unexpected, result of our observations is the discovery of significant absorption in a second (and possibly a third) high redshift quasar. Similar absorption could have been detected in only four of the six high redshift quasar spectra presented here. This high rate of detection implies that among z=3 quasars X-ray absorption is common, but not universal: the non-detection of absorption in one object out of four gives binomial bounds on the mean number of absorbers to z=3 of 0.4−0.9 (90% confidence). The study of high redshift X-ray absorption allows us to investigate physical conditions in the intervening material between us and the quasar, and possibly in the quasar environment. We discuss each of these absorbing possibilities below, after first commenting on the derived spectral indices.

3.1 No change in X-ray slope with luminosity or redshift.

A redshift of three corresponds to a look back time of 75% the age of the universe (for $\Omega_0 = 0$; 67% for $\Omega_0 = 1$). During this time the quasar luminosity function shifted upward in luminosity by a factor ~ 100 in the optical (Boyle *et al.* 1987), and a factor ~ 50 in X-ray luminosity (Boyle *et al.* 1993). Spectral changes in the quasar continuum between local quasars and z=3 would seem inevitable. For example, in the standard scenario of accretion onto a black hole, a large change (>100) in L/L_{Edd} for quasars is implied if it is assumed (admittedly naively) that the observed luminosity evolution is followed by individual quasars [2] (i.e. assuming that they are rare but long-lived). The z=3 quasars we have observed are ~100 times more luminous than those studied by *Ginga*, and so represent the early form of the *Ginga* quasars in the long-lived picture. Alternatively, if quasars are common but short-lived they will most likely remain near the Eddington luminosity and no spectral evolution need be expected. Changes in X-ray slope with redshift were first searched for by

[2]Note that, with these assumptions, $\dot{m}$ decreases toward the present by a factor 50-100 and, since M can only increase, L/L_{Edd} must decrease as z decreases.

Canizares and White (1989) using *Einstein* IPC data. The limited signal-to-noise available prevented any strong constraints being placed. The ROSAT data allow us to revisit this question.

Previously published X-ray spectral slopes for low redshift quasars are plotted as open symbols in figures 5a and 5b as a function of the redshift and of the 2−10 keV luminosity L_{2-10}. These slopes are 1.7−18 keV spectral indices from *Ginga* observations (Williams *et al.* 1992). The errors on the indices plotted are $\pm 1\sigma$ for one interesting parameter, as listed in Williams *et al.* (1992). The *Ginga* data appear to show a flattening with redshift but, as Williams *et al.* show, this is a secondary effect of the well-known difference in mean slope between radio-quiet and radio-loud quasars (Wilkes and Elvis 1987). This can be seen by comparing the two types (radio-quiet are plotted as circles while radio-loud are plotted as squares). The observed range of luminosities for radio-loud quasars alone is only one and a half decades in Williams *et al.* (1992), so it is unsurprising that no dependence is seen. The ROSAT data now extend this analysis to higher luminosities and redshifts.

The ROSAT PSPC spectral indices for our four quasars are plotted as filled symbols in figures 5a and 5b. For the two objects which show intrinsic absorption we have plotted the spectral index obtained allowing both intrinsic N_H and α_E to vary, while for the other two objects we plot the spectral index obtained fixing N_H to the Galactic value. The uncertainties on the PSPC slopes are comparable with those of *Ginga*. The mean PSPC spectral index for the four high redshift radio-loud quasars is 0.71 ± 0.08, well within the 90 % confidence range of Williams *et al.* (1992) for radio-loud quasars of 0.56 − 0.86. Figures 5a and 5b can also be extended to lower luminosities and redshifts using *Ginga* and *EXOSAT* results on broad line radio galaxies. Four such radio galaxies have X-ray spectra in the same ∼1−10 keV rest frame energy range (references are given in the figure caption) and these are plotted in figures 5a,b as triangles (3C390.3 has two measurements). The mean spectral index of these four radio galaxies is 0.61 ± 0.02, which is also consistent with the spectral indices found both in the *Ginga* and ROSAT radio-loud quasars.

No change in the mean rest frame 1−10 keV spectral index greater than 0.3 is detected (at the 99 % confidence level) in either plot. There is no significant correlation in our data between the X-ray spectral indices of radio-loud quasars and their redshift or luminosity (the probability for a correlation is 36% and 30%, respectively). This lack of spectral evolution must begin to set limits on models for quasar X-ray production. Short lifetime models for quasars would seem to be favored. Since we have no radio-quiet quasars as yet we can make no statement on their X-ray spectral evolution.

3.2 Consequences of the Lack of Absorption toward Q0420−388

In Q0420−388 our limit on X-ray absorption is significantly lower than in PKS0438−436 and PKS2126-1158, although it could still be as large as a few 10^{21}

atoms cm^{-2}. This absence of absorption toward one quasar shows that the observed absorption is not universal and so not due to a uniform intergalactic medium. In fact the limit on the X-ray absorption can be turned into a limit on the density of such a medium analogous to the Gunn-Peterson test for Lyman-α (Gunn and Peterson 1965, Peebles 1993). The X-ray version of this test remains sensitive even for high temperatures (10^{6-7}K) where the Lyman-α test loses power (Shapiro and Bahcall 1980). In this way it complements both the Lyman-α test and the COBE limits on the Compton 'y-parameter', which limits the density of a hot ($> 10^8$K) IGM. To apply the X-ray Gunn-Peterson test is however complicated both by the assumptions about the thermal history and metallicity of the IGM, and by the limited spectral resolution of proportional counters. We thus defer discussion of this limit to a later paper.

3.2.1 The Ionization State of Damped Lyman-α Systems.

Damped Lyman-α systems have large column densities of neutral hydrogen compared to other types of quasar absorption lines. They are often considered to be due to extended disks of galaxies at an early stage of evolution (Wolfe 1988). The physical conditions of the absorbing gas are poorly determined from absorption line studies (Lanzetta *et al.* 1991, and references therein). A basic parameter is the ionization state of the gas. In damped Lyman-α systems the fraction of neutral hydrogen is not easily determined. Once the ionization state is determined the presence of an ionizing background radiation can be used to set bounds on the density, size and mass of the absorbing material. Since the X-ray absorption cross-section is relatively insensitive to ionization and depletion (Morrison and McCammon 1983), X-ray measurements give a total column density and so can limit the ionization state of Lyman-α systems.

Q0420−388 has two damped Lyman-α systems in its optical spectra and our limit on X-ray absorption toward this quasar allows us to provide a direct observational limit on their state. The absorbers (which are close to the quasar emission line redshift, at z∼3.08, Atwood, Baldwin and Carswell, 1985) have a total N(HI)=$5 \times 10^{19} cm^{-2}$. Our upper limit on any absorption from them is N(H)=$3.4 \pm 3.3 \times 10^{21}$ atoms cm^{-2}. This gives a lower limit on the neutral to total hydrogen ratio, N(HI)/N(H)>0.004 (3σ), which is quite low. For non-solar metal abundances, which may be 1/10 or lower in damped Lyman-α systems, the implied X-ray hydrogen column density can increase by up to a factor of ∼4 (§2. figure 3), in which case N(HI)/N(H)>0.001.

Another limit to the neutral fraction of hydrogen in these systems comes from the Atwood, Baldwin and Carswell detection of SiII in the damped Lyman-α systems, with a total column of N(SiII)=6.3×10^{15} atoms cm^{-2}. Assuming a solar abundance (Si/H)=$10^{-4.43}$ (Morrison and McCammon 1983), the Si column density corresponds to N(H)=1.7×10^{20} atoms cm^{-2}, so N(HI)/N(H)<0.27. This is an upper limit since

there can be Si in other ionization states which are not currently detectable, and Si may have lower abundance, thus increasing the implied N(H).

Lanzetta *et al.* (1991) find that the integrated amount of neutral material in all damped Lyman-α systems can account for Ω_0=1, so that statistically the amount of ionized material cannot exceed this by more than a factor of a few. In contrast, our X-ray measurement is a direct limit for a particular system.

The above neutral fraction limit can be converted into a limit on size and density, given an assumed background ionizing radiation field, J(912Å). As an example we have taken J(912Å)=10^{-21}erg cm^{-2} s^{-1}Hz$^{-1}Sr^{-1}$ (Lu, Wolfe and Turnshek 1991, Bajtlik, Duncan and Ostriker, 1988) and solar abundances. This leads only to a weak limit on the size and density of the absorbing material, < 3Mpc, and > 10^{-3}cm^{-3} (figure 6).

The value of J(912Å) used is a lower limit to the ionizing flux experienced by the absorber. The damped systems are close to the "proximity effect" Stromgren sphere of the quasar, so the UV radiation from the quasar may be as important as the metagalactic flux depending on the latter's value. The clouds are also expected to be in a galactic environment and so are likely to be subject to a strong stellar radiation field. Finally, unlike the Lyman-α forest clouds, the damped systems are unlikely to be solely photoionized. Qualitatively, all these factors move the limits on size and density toward smaller, denser clouds.

The size limit also depends sensitively on the X-ray column density. For a limit on $N_H < 10^{21}$ atoms cm^{-2} this limit would become < 25 kpc (figure 6), and so would constrain the absorber to no more than galaxy-like dimensions. Such a limit should be readily attainable with soft X-ray instrumentation. (Although the PSPC itself is not likely to be available for long enough for such an observation to be performed.)

3.3 High Redshift X-ray Absorption

The appearance of large amounts of absorption in the X-ray spectra of high redshift quasars is surprising in two ways. First, these quasars have strong blue ultraviolet continua that give no hint of large amounts of obscuration; second heavy obscuration has been rarely reported in high X-ray luminosity AGN at low redshift. We first discuss these two points, and then go on to consider possible intervening and intrinsic sites for the absorbers.

The lack of ultraviolet reddening has implications for the amount and distribution of dust in the absorber. For standard Milky Way values of the interstellar dust-to-gas ratio an HI column density of 10^{22} atoms cm^{-2} corresponds to $A_V \sim 4$. As Bechtold *et al.* (1993) will discuss, a value of $A_V > 0.5$ is highly unlikely to be affecting the ultraviolet spectrum of these quasars. There are several possibilities to explain this apparent contradiction: (1) The metal abundances at z=3 could be much reduced so that a large N_H does not correspond to a large metal, and hence

dust, column; (2) the dust-to-gas ratio in the absorber may be much lower than in the Milky Way; (3) the dust in the absorbers may contain only large grains that do not cause reddening (see *e.g.* Laor and Draine 1993); (4) The absorber may have a geometry that obscures only the X-ray source and not the ultraviolet source, in which case it must originate close to the active nucleus.

We argue below that (4) is unlikely. In cooling flows, a possible site for the absorber (see §3.3.2), X-ray sputtering may well destroy small grains (see White *et al.* 1991, and references therein), so that (3) can have some physical justification. The dust-to-gas ratio in damped Lyman-α systems is much debated because of its importance to quasar visibility at high redshifts, and its importance for early galaxy evolution (see Fall and Pei, 1993, and references therein). Pei, Fall and Bechtold (1991) show that, for Milky Way type dust, this ratio must be no more than 1/10 the Milky Way value. Others have suggested that the metal abundances in damped Lyman-α systems is no more than 1/10 solar (Meyer and Roth 1990, Pettini, Boksenberg and Hunstead 1990, Turnshek *et al.* 1989). Possibilities (1) and (2) are therefore plausible for intervening systems.

X-ray absorption in quasars of high X-ray luminosity is highly unusual, column densities $< 5 \times 10^{20}$ atoms cm^{-2} being normal (Wilkes and Elvis 1987, Kruper, Urry, and Canizares, 1990, Williams *et al.* 1992). In figures 7a,b we show a plot of excess absorption against redshift and X-ray luminosity compiled from *Ginga* , *Einstein* and ROSAT measurements. (References are given in the figure caption.) From figure 7 it is clear that at low X-ray luminosities ($< 10^{44} erg\ s^{-1}$) large X-ray column densities are common in AGN (Lawrence and Elvis 1982, Turner and Pounds 1989), while above $10^{44} erg\ s^{-1}$ a clear drop in the number of absorbed systems can be seen. Note that this drop is not due to insensitivity to column density by *Ginga*, or *Einstein*, nor is it due just to small number statistics. (There are more than 20 quasars in this range. The binomial probability of finding 3 out of 4 absorbed when 1 in 20 is expected is 0.0005.) The high redshift ROSAT results reverse this trend. (Recall that both *Ginga* at low redshift, and ROSAT at high redshift, are sensitive to the same emitted energy range.) Is a new mechanism is needed to produce the absorption detected at high z and/or luminosity, or can known low z absorbers suffice? First we consider the two previously suggested sites for absorption in AGN - the broad emission line region, and jets. We find that these are unlikely to apply to the high redshift quasars.

Since the absorption in low luminosity AGN is time variable it is normally associated with the environs of the broad emission line region. That the cases of absorption seen above a luminosity of 10^{44} erg s^{-1} at low z are 'warm' (*i.e.* partially ionized, see figure 7 open circles) suggests that this site becomes too ionized by the continuum to be effective at higher luminosities. An evolutionary change in the broad emission line region could be invoked, but the emission lines of quasars show no striking changes with redshift (Schneider, Schmidt and Gunn 1989).

Cool material in a relativistic jet may appear implausible, yet X-ray absorption is seen in several BL Lac objects (Canizares and Kruper 1984, Madejski *et al.* 1991) and in the OVV NRAO140 (Marscher 1988). Since PKS0438−436 is a strong, core dominated, radio source it is likely to be relativistically beamed towards us, leading Wilkes *et al.* (1992) to suggest that the absorbing material may be located within the radio emitting jet. However, neither PKS0438−436 nor PKS2126−158 are clearly blazars, since neither has polarization that is convincingly above the 3% threshold that is normally used to indicate blazar-like activity (Impey and Tapia 1990). For PKS0438−436 Impey and Tapia (1990) report 4.7±1.0%, but Fugmann and Meisenheimer (1988) find only 1.6±0.5%. Wills *et al.* (1992) report an optical polarization of only 1.7±0.9% for PKS2126−158.

More tellingly, PKS2126−158 and S4 0636+680 are Gigahertz Peaked Spectrum (GPS) radio sources. Beaming is not believed to be important in GPS sources because of their low radio polarization, steep high frequency spectra, and lack of strong variability (O'Dea, Baum and Stanghellini 1991).

Since beaming is probably unimportant, the large derived X-ray luminosities of the GPS quasars PKS0420−388 and PKS2126−158 are thus likely to be true 4π values (Phillips and Mutel 1982). Such luminosities imply extreme masses ($\sim 10^{10-11} M_{\odot}$) for the presumed massive black holes at their centers, and predict strong limits on any X-ray variability ($\sim$ 1 year, quasar frame).

The reappearence of absorption at luminosities above $10^{46} ergs^{-1}$ and/or at redshifts greater than one in the ROSAT PSPC data suggests that a different mechanism may be coming into play. Since the broad emission line region and jets are unlikely, we are forced to examine other sites, further from the nucleus. We next consider the possibility that the absorption is unconnected with the quasar, merely lying along the line of sight; and then go on to consider an origin in the quasar environment on a galaxy or cluster of galaxies scale.

3.3.1 Intervening Absorbers: Damped Lyman-α Systems?

Since the PSPC energy resolution does not allow us to determine the redshift of the absorption, it may also lie anywhere along the line of sight between our galaxy and the quasar. Absorption would then be seen primarily in high z quasars simply because they have a longer path length along which an absorber might lie. The path length for absorption for a uniformly distributed population of absorbers is given by the co-ordinate X (in units of c/H_0, Wagoner 1967, Bahcall and Peebles 1969) which allows for the increased crowding of objects at z increases. ($X=0.5[(1+z)^2 - 1]$, $\Omega_0=0$; $X=\frac{2}{3}[(1+z)^{3/2}-1]$, $\Omega_0=1$.) Figure 8 shows the absorption path length, X, toward our z=3 quasars PKS0438−436 and PKS2126−158. The lack of absorption toward quasars at z∼0.3−0.4 (Wilkes and Elvis 1987) excludes only a small region near the origin. At z=3 X is 22 times larger than at z=0.3 (for $\Omega_0=0$, 15 times for $\Omega_0=1$), so a 5% chance of an intervening system in the low redshift objects becomes

close to unity by z=3, if there is no evolution in the mean free path for absorption. This makes an intervening explanation seem quite natural.

In the context of intervening absorbers the sensitivity of X-ray absorption to higher Z elements makes the abundances and the ionization state of the absorbers critical to an assessment of the probability that a particular absorption system causes the X-ray absorption. The ionization states are often poorly known from optical and ultraviolet absorption lines since these lines sample only a limited number of elements and ions. Conversely, given a redshift, X-ray absorption data can be used to determine or limit the ionization fraction (as in §3.2).

There are four major classes of candidate intervening absorbers in the optical spectra of quasars (Sargent 1988). In order of increasing column density they are: Lyman-α forest lines ($\sim 10^{12-16}$atoms cm^{-2}); Lyman limit systems ($\sim 10^{>17}$atoms cm^{-2}); Metal line systems ($\sim 10^{>16}$atoms cm^{-2}); and damped Lyman-α systems ($\sim 10^{19-21}$atoms cm^{-2}). If sufficiently highly ionized, absorbers of almost any type might produce the observed X-ray absorption. However, the damped Lyman-α absorbers are the most straightforward to associate with the X-ray absorption due to their large N(HI) values (Sargent 1988, Wolfe 1988).

Neither of the well-determined X-ray absorbers shows any intervening damped Lyman-α system at z>1.88 (Morton, Savage and Bolton 1978, Sargent, Steidel and Boksenberg 1990, Lanzetta, Turnshek and Wolfe 1987) [3]. This eliminates half of the available absorption path length for damped Lyman-α absorption systems (figure 8). Below this redshift Lyman limit systems in both quasars cut out all emission, so no other absorption systems can be detected. The Lyman limit system in PKS2126−158 has a column density of N(HI)$> 2-3\times10^{17}$ atoms cm^{-2} (Sargent, Steidel and Boksenberg 1990), and has no associated Lyman-α. PKS0438−436 has not been studied for absorption systems. If this were the origin of the absorption we see it implies N(HI)/N(H)$< 3\times10^{-5}$.

Given the number density of absorbers per unit redshift, dN/dz, of Lyman-α absorption systems with large HI column density we can derive the probability of finding two such absorbers at z<1.88 toward to two out of three quasars.

$$\frac{dN}{dz} = \sigma\rho_0(1+z)(1+2q_0z)^{-1/2},$$

where σ is the cross-section of the absorbers, and ρ is their space number density. Empirical fits to dN/dz are usually made assuming: $dN/dz = A_0(1+z)^\gamma$, where A_0 and γ are constants. For Ω_0=0 and no evolution γ=1, while for Ω_0=1 and no evolution γ=1/2. Lanzetta *et al.*(1991) have two samples for which they find: A_0= 0.035, γ=1.2±1.7; A_0= 0.163, γ=0.3±1.4. Errors in A_0 and γ are highly correlated, so for simplicity we assume that the major uncertainty is in γ. Integrating these empirical fits over 0<z<1.88, assuming no evolution, gives an expected number of systems

[3] A possible NaD line in the spectrum of PKS2126−158, which would imply extremely low ionization and so a large column density, is not confirmed in a spectrum taken by one of us (JB).

of 0.147 and 0.371 respectively. Within the uncertainties the predicted numbers of absorbers are consistent with the mean of 0.4-0.9 X-ray absorbers per z=3 quasar that we find. For 0<z<0.5 these numbers are much smaller, 0.023 and 0.087, so that not seeing absorbers in the X-ray spectra of low redshift quasars (Wilkes and Elvis 1987) is also consistent with an intervening explanation.

The X-ray case is somewhat more complicated than that for Lyman-α since σ is energy and abundance dependent. Figure 4 shows that for a given N_H the cut-off in the X-ray spectrum declines as $z_{absorber}$ increases, roughly as (1+z). Figure 3 shows primordial material has a σ about 1/4 that of solar material. The dependence of σ on z and abundances makes it understandable how the high z damped Lyman-α absorber in Q0420−388 can not strongly affect the PSPC spectrum, while lower z systems with the same N(HI) would produce an X-ray cut-off.

There are three unknowns: the evolution of high column density absorbers toward low redshift; the ionization state of these absorbers; and their abundances. Lower space densities for nearby absorbers would make an intervening explanation less likely. The space density of damped Lyman-α systems below $z\sim2$ has not been studied to date because of the limited path length to any one object, so that large samples are needed to make strong statements. A decline in numbers toward the present is allowed. Models that ascribe the damped Lyman-α systems to haloes of protogalaxies must have a strong reduction in their space densities toward low redshift (Wolfe 1988). The use of z=2 densities at lower redshifts thus requires a large extrapolation. A higher ionization level would enable absorbers with lower neutral N_H to produce the observed X-ray column, thus raising the total number of absorbers available. To produce a X-ray column density of $1-5\times10^{21}$ atoms cm^{-2}, an absorber with solar metal abundances and N(HI)=$1-5\times10^{20}$ atoms cm^{-2} would need N(HI)/N(H) = 10^{-1}. This is within our own limit on N(HI)/N(H) for Q0420−388 (§3.2). Since dN/dz rises with a slope of 1.8 to lower N(HI) even a factor 4 higher ionization fraction would give 12 times the number of expected absorbers.

Thus for both quasars intervening damped Lyman-α systems can plausibly produce the X-ray absorption. However the argument is statistical, and it is worthwhile to consider alternative explanations.

3.3.2 Intrinsic Absorption: Intracluster gas at z=3?

The large look back time to redshift 3 allows plenty of scope for evolutionary changes in the host galaxy and in the larger scale environment. Most of the potential changes are not yet theoretically well-developed however. An origin related to cluster environment is plausible, since all the observed quasars are radio-loud, and at z>0.7 radio-loud quasars tend to be found in rich galaxy environments (Yee and Green 1984, Ellingson, Yee and Green 1991). In hierarchical biased CDM scenarios clusters of galaxies are predicted to form at the peaks of initial density fluctuation at $z\gtrsim2$ (Kaiser 1984, Davis et al. 1985). Optical searches for distant clusters reveal several

dense cores which are already relaxed (i.e. have high velocity dispersions $\langle v^2 \rangle^{1/2} \gtrsim 10^3$ km s^{-1} and nearly homogeneous galactic populations) at $z \gtrsim 0.7$ (Gunn 1990, Ellis 1992) thus suggesting the presence of hot and dense gas at those z.

The presence of Gigahertz Peaked Spectrum sources in our sample suggests an intriguing possibility for the site of the absorbers in these high redshift quasars. GPS sources are unusually compact (~10 milliarcsec, ~ 100 pc at z=3, Pearson and Readhead 1984). This compactness likely implies a dense surrounding medium to confine the radio source. A cooling flow around the quasar provides a plausible mechanism and could also explain the absorbing columns that we have detected.

The pressures needed to produce the low frequency cut off in the radio spectrum due to free-free absorption are $\sim 10^8 cm^{-3} K$ (O'Dea *et al.* 1991). These are similar to the pressures in an X-ray cooling flow on a quasar (Fabian and Crawford 1990). Thermal confinement of the GPS sources had been considered unlikely by O'Dea *et al.* (1991) because the amount of cold ($T \sim 10^4 K$) material needed is excessive. The presence of gas at X-ray temperatures would remove this problem and would tie together two key properties of GPS sources: confinement and low frequency cut-offs. A cooling flow could also lead to a synchrotron self-absorption cut-off by keeping the radio source unusually compact. Neutral hydrogen has been detected in absorption against a radio galaxy at z=3.4 (B2 0904+343, Uson, Bagri and Cornwell, 1991) with an HI column density of $\sim 4.4 \times 10^{18}\ T_s$ atoms cm^{-2}, where T_s is the spin temperature of the HI. T_s could have a value of $\sim 10^4$ (Uson *et al.* 1991), so the total hydrogen column could be of the correct order of magnitude to be related to our X-ray absorbers.

At low redshifts X-ray absorption from material associated with cooling flows has been detected with column densities up to a few 10^{21} atoms cm^{-2} (White *et al.* 1991), within a factor of a few as large as those seen in PKS043S−436 and PKS2126−158. These column density values have been obtained assuming an uniform absorbing screen. The absorbing gas, however, is likely to be clumpy and mixed with the hot emitting gas. Active nuclei are small so that absorption toward them could well pass through only one cloud, and so record somewhat larger N_H values than the averaged values provided by the extended hot gas in a cluster core. There is consistency with the low redshift AGN seen at the centers of cooling flows which do in fact have similarly large X-ray column densities (NGC1275, Fabian *et al.* 1981; M87 Schreier *et al.* 1982; Cygnus A, Arnaud *et al.* 1987), as do however, many AGN not in cooling flows. Thus the X-ray absorption we see in high redshift quasars may represent the detection of intracluster material at z~3.

The fact that our quasars were selected to be among the most luminous known could bias us toward objects in strong cooling flows. Fabian and Crawford (1990) have pointed out that the quasar continuum emission will Compton cool the material in a cooling flow, and so may increase the quasar accretion rate in a feedback that

enhances the quasar luminosity. The most luminous quasars may thus be found in the strongest cooling flows.

One candidate GPS quasar, Q0420−388, does not show excess absorption. This does not in itself constitute evidence against the absorption in the high z quasars being related to cooling flows. White *et al.* (1991), with better sensitivity to absorbing column densities than in our data, find excess absorption in only 12 out of 21 clusters. None of the three quasars with X-ray absorption has a damped Lyman-α or Lyman limit systems near the quasar emission redshift (Sargent, Steidel and Boksenberg 1990, Morton, Savage and Bolton 1978), although PKS0438−436 does have three narrow Lyman-α absorption lines superimposed on the Lyman-α emission line. If the X-ray absorber is at z(em), it must be highly ionized (N(HI)/N(H) $< 10^{-5}$). The quasar continuum will photoionize a region around the quasar that could well encompass the whole cooling flow region.

The X-ray continuum emission from any putative cluster or cooling flow is not likely to be a strong contaminant of the quasar spectrum. The highest X-ray luminosity known from a cluster of galaxies is $6.4 \times 10^{45} erg\ s^{-1}$ (2-10 keV) for A2163 (Arnaud *et al.* 1992). This extreme cluster would contribute no more than 10% to the flux of Q0420−388, or 0.7% of PKS2126−158. An arcsecond resolution X-ray image would be able to directly resolve such cooling flows.

A cooling flow is not the only possible site for intrinsic absorption due to a cluster. Uson *et al.* (1991) also found extended HI emission at the same redshift as the absorption but 33 arcminutes away. This emission requires a large mass, and narrow line width implies a non-virialized mass near turnaround (*i.e.* just separating from the Hubble flow), possibly a Zel'dovich pancake (Uson *et al.* 1991), or cluster of galaxies (Subramanian and Swarup, 1992). The HI column density of this 'protocluster' is similar to that seen in our quasar X-ray spectra at similar redshifts, and an identification of such material with our absorbers may imply significant metal abundances in the 'protocluster' material. Subramanian and Swarup associate this HI with that of the damped Lyman-α systems, so that the same statistics used above apply to this explanation. However the lack of damped Lyman-α systems near the emission redshift in any of the high z quasars with evidence for X-ray absorption, mentioned above, limits the ionization state and/or geometry of the 'protocluster'.

3.4 Fe-K Lines

Low redshift broad emission line AGN emit strong Fe-K 6.4 keV fluorescence lines (equivalent width of 50-300 eV, Nandra *et al.* 1991). In addition, if the z$\sim$ 3 quasars are surrounded by dense hot gas, they will show strong Fe-K 6.5-7 keV lines (1000 eV equivalent width, with respect to the *thermal* continuum), and if the absorption of X-rays is due to intracluster gas, this will also produce an additional fluorescence line. The limits we derive for the Fe-K 6.4 keV fluorescence indicate that with moderately improved sensitivity iron K lines measurements of high redshift

quasars will begin to constrain models. The Gas Scintillation Proportional Counters and the CCDs which will be on board *Asuka*, SAX and SPECTRUM X$-\gamma$ will probably be capable of detecting these lines, since the lines will fall at 1$-$2 keV where all these missions have their greatest effective area.

4. CONCLUSIONS

We have presented X-ray spectral data for six z=3 quasars. Three of them show evidence for excess absorption along the line of sight above the Galactic value at $\sim 10^{22}$atoms cm^{-2} (at the quasar redshift, for solar abundances). In two others such a column could not be detected due to the large Galactic column density. Only one quasar clearly has a lower level of absorption. We conclude that X-ray absorption is a common, but not universal, property of high redshift, radio-loud quasars. The UV continua of these quasars show no sign of strong absorption.

Two explanations are at present equally plausible, one intervening and one intrinsic. If the detected X-ray absorption is due to intervening systems, then damped Lyman-α absorbers at $0.3 < z < 1.9$, are the prime candidates. Damped Lyman-α absorbers can have sufficient column density, and may have sufficient space density. However this requires an extrapolation because the density of damped Lyman-α systems at redshifts below 2 is unknown.

If the absorption is intrinsic it is not likely to be associated with a jet, nor with the broad emission line region. A possible site for the X-ray absorption lies in cold material in intracluster gas, for example a cooling flow, around the quasars. This material may cause the Gigahertz peaked radio spectrum in two of the objects, through either free-free absorption or synchrotron self-absorption, due to the increased compactness. Intracluster material may also be linked to the extreme luminosity of these objects through enhancement of the accretion rate due to Compton cooling of the flow by the quasar continuum. Absorption by a Zel'dovitch pancake or protocluster is another possibility, which may imply a lower bound on the enrichment of the material and/or limit the geometry of the material.

The quasar with no detected X-ray absorption has no known intervening damped Lyman-α absorbers. The X-ray measurement implies a limit on the neutral fraction for these systems, N(HI)/N(H)$> 4 \times 10^{-3}$ (3σ), for solar abundances, and a size of <3Mpc.

The lack of an X-ray redshift prevents us from knowing whether, with X-ray absorption toward high redshift quasars, we are studying clusters at z=3 or disk galaxies (the preferred explanation for damped Lyman-α systems) at z$\sim$ 1. High resolution spectroscopy around the redshifted Oxygen K-edge (0.2-0.5 keV) is the most promising diagnostic. Also high resolution (arcsecond) X-ray imaging could separate a quasar from any surrounding cooling flow.

We compared the 1$-$10 keV (emitted) spectral indices of the z=3 quasars

with spectra in the same emitted energy range from low z radio-loud quasars. They show no evidence for changes in X-ray slope greater than 0.3 (99% confidence), either between z=0.1 and z=3, or from $L_X = 10^{44} erg\ s^{-1}$ to $L_X = 10^{48} erg\ s^{-1}$. This tends to favor short lifetime models for quasars.

Limits of 0.7−1.5 keV were placed on the equivalent width of the Fe-K 6.4 keV fluorescence emission for all four objects.

The large derived X-ray luminosities of two of these quasars (the GPS quasars PKS0420−388 and PKS2126−158) are likely to be true 4π values, unaffected by relativistic beaming. Such luminosities imply extreme masses ($\sim 10^{10-11} M_\odot$) for the presumed massive black holes at their centers, and predict strong limits on any X-ray variability ($\sim$ 1 year, quasar frame).

ACKNOWLEDGMENTS

We thank Sergio Colafrancesco for discussions on cluster formation scenarios. We also thank Mark Birkinshaw, Pepi Fabbiano, Harvey Tananbaum, and the referee, Claude Canizares, for critical readings of the manuscript. This research has made use of the NASA/IPAC Extragalactic Database (NED) which is operated by the Jet Propulsion Laboratory, California Institute of Technology, under contract with the National Aeronautics and Space Administration. This research has also made use of the Einstein On-Line Service, Smithsonian Astrophysical Observatory. This work was supported by NASA grants NAGW-2201 (LTSARP), NAG5-1872 and NAG5-1536 (ROSAT), and NASA contracts NAS5-30934 (RSSDC), NAS5-30751 (HEAO-2) and NAS8-39073 (ASC).

REFERENCES

Allen S.W., and Fabian A.C., 1992, MNRAS, 258, 29p.
Arnaud K.A., *et al.* 1987, MNRAS, 227, 241.
Arnaud, M., Hughes, J.P., Forman, W., Jones, C., Lachieze-Rey, M., Yamashita, K., and Hatsukade, I. 1992, ApJ, 390, 345.
Atwood B., Baldwin J.A., and Carswell R.F.,1985, ApJ, 292, 58.
Awaki H. 1992 PhD thesis.
Bahcall J. and Peebles J., 1969, ApJ, 156, L7.
Bajtlik S., Duncan R. C., Ostriker J. P., 1988, ApJ,327, 570.
Bechtold J., *et al.* 1993, in preparation.
Boyle B.J., Fong R., and Shanks T. 1987, MNRAS, 227, 717.
Boyle B.J., Griffiths R.E., Shanks T., Stewart G.C., and Georgantopoulos I. 1993, MNRAS, 260, 49.
Canizares C.R., and Kruper J., 1984, ApJ, 278, L99.
Canizares C.R., and White J.L., 1989, ApJ, 339, 27.

Condon J.J., Condon M.A., Jauncey D.L., Smith M.G., Turtle A.J., Wright A.E., 1981, ApJ, 244, 5.
Davis, M., Efstathiou, G.G., Frenk, C.S., and White, S.D.M. 1985, ApJ, 292, 371.
Ellingson E., Yee H.K.C. and Green R.F., 1991, ApJS, 76, 455.
Ellis, R.S. 1992, in *"The Stellar Population of Galaxies"*, B. Barbuy and A. Renzini Eds., p. 297.
Elvis M., Lockman F.J. and Wilkes B.J. 1989, ApJ, 97, 777.
Elvis M., Wilkes B.J., McDowell J. C., Green R.F., Bechtold J., Willner S.P., Oey M.S., Polomski E., and Cutri R., 1993, ApJS, *submitted.*
Fabian A.C., Hu E.M., Cowie L.L., and Grindlay J. 1981, ApJ, 248, 47.
Fabian A.C. and Crawford C.S., 1990, MNRAS, 247, 439.
Field G.B., and Perrenod S.C., 1977, ApJ, 215, 717.
Fiore F, Perola G.C., Matsuoka M., Yamauchi M., and Piro L. 1992, A&A., 262, 37
Fiore F., Elvis M., Mathur S., Wilkes B.J., and McDowell, 1993, ApJ, in press (September 20).
Fireman E.L., 1974, ApJ, 187, 57.
Fugmann W. and Meisenheimer K. 1988, A& AS, 76, 145.
Giallongo E., Cristiani S., and Trevese D., 1992, ApJ, 398, L9.
Gunn, J.E. 1990, in *"Clusters of Galaxies"* (Cambridge: Cambridge Univ. Press), p. 341
Gunn J.E. and Peterson B. A., 1965, ApJ, 142, 1633.
Halpern J.P. 1984, ApJ, 281, 90.
Harris D.E. *et al.* 1990, "The Einstein Observatory Catalog of IPC X-ray Sources", CD-ROM, *Einstein* Data Center, Smithsonian Astrophysical Observatory.
Hasinger G., and Snowden 1992, priv. comm.
Heiles C. and Cleary M.N., 1979, Aust. J. Phys. Suppl., 47, 1.
Hyland A.R., and Allen D.A., 1982, MNRAS, 199, 943.
Impey C. and Tapia S. 1990, ApJ, 354, 124.
Inda A., Makishima K., Kohmura Y., Tashiro M., Ohashi T., Barr P., Hayashida K., Palumbo G.G.C., Trinchieri G., Elvis M., and Fabbiano G., 1993, ApJ, submitted.
Jauncey D.L., Wright A.E., Peterson B.A., and Condon J.J., 1978, ApJ, 223, L1.
Kaastra J.S., Kunieda H. and Awaki H. 1991, A&A, 242, 27.
Kaiser, N. 1984, ApJ(Letter), 284, L49.
Kühr H., Witzel A., Pauliny-Toth I.I.K., and Nauber U., 1981, A& AS, 45, 367.
Kruper J.S., Urry C.M., and Canizares C.R., 1990, ApJS, 74, 347.
Laor A. and Draine B.T., 1993, ApJ, 402, 441.
Lanzetta K.M., Wolfe A.M., Turnshek D.A., Lu L. McMahon R.G., and Hazard C., 1991, ApJS, 77, 1.
Lanzetta K.M., Turnshek D.A., and Wolfe A.M., 1987, ApJ, 322, 739.
Lawrence A., and Elvis M., 1982, ApJ, vol256, 410.
Lawson A.J., Turner M.J.L., Williams O.R., Stewart G.C. and Saxton R.D. 1992,

MNRAS, 259, 743.
Lu L., Wolfe A. M., Turnshek D.A., 1991, ApJ, 367, 19.
Maoz D., Bahcall J.N., Doxsey R., Schneider D.P., Bahcall N.A., Lahav O., and Yahalay B., 1992, ApJ, 394, 51.
Madejski G.M., Mushotzky R.F., Weaver K.A., Arnaud K.A., and Urry C.M., 1991, ApJ, 370, 198.
Marscher A.P. 1988, ApJ, 334, 552.
Marshall F.E., Netzer H., Arnaud K.A., Boldt E.A., Holt S.S., Jahoda K.M., Kelley R., Mushotzky R.F., Pierre R., Serlemitsos P.J., Smale A.P., Swank J.H., Szymkoviak A.E., and Weaver K.A., 1993, ApJ, 405, 168.
Mather J.C., *et al.*, 1990, ApJ, 354, L37.
Meyer D.M., and Roth K.C., 1990, ApJ, 363, 57.
Morrison R. and McCammon D., 1983, ApJ, 270, 119.
Morton D.C., Savage A., and Bolton J.G. 1978, MNRAS, 182, 735.
Nandra K., Pounds K.A., 1992, Nature, 356, 215.
Nandra K., Pounds K.A., Stewart G.C., 1991, in "Iron Line Diagnostics in X-ray sources", eds. A. Treves, G.C. Perola and L. Stella [Berlin:Springer-Verlag], p.177.
Nandra K. 1992, PhD thesis.
O'Dea C.P., 1990, MNRAS, 245, 20P.
O'Dea C.P., Baum S.A., and Stanghellini C., 1990, ApJ, 380, 66.
Osmer P. S. Smith M.G., 1977,ApJ. Letters, 2 [illegible]47.
Pan H.C., Stewart G.C. and Pounds K.A. 1990, MNRAS, 242, 177.
Pearson T.J., and Readhead A.C.S., 1984, IAU Symposium no. 110, "VLBI and Compact Radio Sources", [Dordrecht:Reidel], p. 15.
Peebles P.J.E., 1993, *Principles of Physical Cosmology*, [Princeton:Princeton Univ. Press], p. 550.
Pettini M., Boksenberg A., and Hunstead R.W., 1990, ApJ, 348, 48.
Fall M., and Pei Y., 1993, ApJ, 402, 479.
Pei Y., Fall M., Bechtold J., 1991, ApJ, 378, 6.
Peterson B.A., Savage A., Jauncey D.L. and Wright A.E., 1982, ApJ, 260, L27.
Pfefferman E., *et al.* 1987, Proc. SPIE, 733, 519.
Phillips R.B., and Mutel R.L., 1982, A& A, 106, 21.
Pounds K.A. 1990, MNRAS, 242, 20p.
Raymond J., and Smith B.W., 1977, ApJS, 35, 419.
ROSAT Mission Description, 1991, NASA NRA 91-OSSA-3, Appendix F.
ROSAT Newsletter no. 10., 1992.
Rybicki G.B., and Lightman A.P., 1979, *Radiative Processes in Astrophysics*,[New York:Wiley]
Sargent W.L.W., 1988, in "QSO Absorption Lines", eds. J.C. Blades, D. Turnshek, and C.A. Norman [Cambridge:CUP], p.1.
Sargent W.L.W. and Steidel C. and Boksenberg A., 1990, ApJ, 351, 364.

Schlegel E., priv. comm.
Schneider D. P., Schmidt M., and Gunn J.E., 1989, AJ, 98, 1507.
Schneider D. P., Bahcall J.N., Saxe D.H., Bahcall N.A., Doxsey R., Golombek D., Krist J., McMaster M., Meakes M., Lahav O., 1992, PASP, 104, 678.
Schreier E.J., Burns J.O., Gorenstein P., and Feigelson E.D. 1982, ApJ, 261, 42.
Shapiro P.R. and Bahcall J.N., 1980, ApJ, 241, 1.
Shastri P., Wilkes B.J., Elvis M., and McDowell J., 1993, ApJ, in press (June 1).
Singh K.P., Rao A.R. and Vahia M.N. 1990, MNRAS, 246, 706.
Stark A.A., Gammie C.F., Wilson R.W., Bally J., Linke R., Heiles C., and Hurwitz, M., 1989, ApJS, 79, 77.
Subramanian K., and Swarup G., 1992, Nature, 359, 512.
Trümper J., 1983, Adv. Space Res., 2, No.4 241.
Turner T.J., and Pounds K.A., 1989, MNRAS, 240, 833.
Turner T.J. and George I.M., 1992, "ROSAT PSPC Calibration Guide", NASA GSFC OGIP Calibration Memo.
Turner, T.J., Done, C., Mushotzky, R., Madejski, G., & Kunieda, H. 1992, ApJ, 391, 102.
Turnshek D.A., Wolfe A.M., Lanzetta K.M., Briggs F.H., Cohen R.D., Foltz C.B., Smith H.E., and Wilkes B.J., 1989, ApJ, 344, 567.
Uson J.M., Bagri D.S., and Cornwell T.J., 1991, Phys. Rev. Lett., 67, 3328.
Veron-Cetty M.-P. and Veron P., 1991, ESO Scientific Report no. 10.
Wagoner R., 1967, ApJ, 149, 465.
White D.A., Fabian A.C., Johnstone R.M., Mushotzky R.F., and Arnaud K.A., 1991, MNRAS, 252, 72.
Wilkes B.J. and Elvis M., 1987, ApJ, 323, 243.
Wilkes B.J., Elvis M., Fiore F., McDowell J.C., Tananbaum H. and Lawrence A. 1992, ApJ (Lett), 393, L1.
Wilkes, B.J., Tananbaum, H., Worrall, D.M., Avni, Y., Oey, M.S. and Flanagan, J. 1993, ApJS, *submitted.*

Wills B.J., Wills D., Breger M., Antonucci R.R.J., and Barvainis R., 1992, ApJ, 398, 454.
Williams O.R. et al., 1992, ApJ, 389, 157.
Wolfe A.M., 1988, in "QSO Absorption Lines", eds. J.C. Blades, D. Turnshek, and C.A. Norman [Cambridge:CUP], p.297.
Worrall D.M., and Wilkes B.J., 1990, ApJ, 360, 396.
Yee H.K.C. and Green R.F., 1984, ApJ, 280, 79.

Figure Captions

Figure 1: ROSAT PSPC pulse height spectra for the four high z quasars. The upper panel in each case shows the pulse height spectrum and best fit power-law plus absorption model, and the lower panel shows the residuals from these fits. The fits shown are (a) S5 0014+813 and (b) Q0420−388: N_H fixed at the Galactic value; (c) PKS0438−436 (coadded spectrum), and (d) PKS2126−158 (coadded spectrum): N_H at the best fit value in the quasar frame.

Figure 2: Contours of allowed values of α_E and N_H for the four high z quasars. The thin solid contours are for z=0 absorption, which can be compared with the Galactic HI values (horizontal dashed lines). The thick contours are for absorption at the quasar redshift. Contours are 68 %, 90%, and 99 % confidence for 2 interesting parameters.

Figure 3: The dependence of the ratio R, the metal abundances relative to the solar value, on N_H at the quasar redshift for PKS0438−436 (filled circles) and PKS2126-158 (empty circles).

Figure 4: The dependence of the deduced equivalent hydrogen density on the redshift assumed for the absorber along the line of sight to (a) PKS0438−436 and (b) PKS2126-158 (solid line). The dashed lines show the 68% confidence region for this absorption.

Figure 5: X-ray energy spectral index in the ∼1−10 keV *emitted* frame vs. (a) redshift, (b) luminosity. Squares represent radio-loud quasars, circles radio-quiet quasars, and triangles radio galaxies. The ROSAT PSPC spectral indices for the four z∼3 quasars are plotted as filled symbols. The other points (open symbols and triangles) are *Ginga* results reported by Williams *et al.* (1992) for the quasars and by various authors for the radio galaxies (3C445, Pounds 1990; Pictor A, Singh, Rao and Vahia 1990; 3C382, Kaastra, Kunieda and Awaki 1991; 3C390.3, Inda *et al.* 1993).

Figure 6: Physical size of the damped Lyman-α system in Q0420−388, versus ionized fraction for a PSPC-derived total column density of $<10^{22}$ atoms cm^{-2} (solid line). The non-linear dependence on the X-ray derived column density is shown with the dashed line that gives the limits in the hypothetical case of a limit of $<10^{21}$ atoms cm^{-2} (dashed line).

Figure 7: Absorbing X-ray column density vs. redshift (a), 2−10 keV luminosity (b).

The upper limits and solid squares below z=0.3 are *Ginga* measurements taken from Awaki (1992), and Nandra (1992) PhD theses. The upper limits and solid squares at z>0.3 are *Einstein* IPC measurements (Wilkes and Elvis 1987, Marscher 1988). Triangles indicate ROSAT measurements and upper limits from this paper and from Allen and Fabian (1992). Open circles indicate likely 'warm' absorbers (from Pan *et al.* 1990, Fiore *et al.* 1992, 1993, Turner *et al.* 1992, Nandra and Pounds 1992).

Figure 8: Possible locations for damped Lyman-α absorbers toward PKS0438−436 and PKS2126−158 as a function of the path length for absorption, X. Previous limits from studies of quasars at z$\sim$0.3-0.4 constrain the absorption very little. No damped Lyman-α systems are found at z>1.88 in either quasar, which rules out half of the available path length for absorption. The presence of Lyman limit systems cut out all information about Lyman-α absorbers at z<1.88 in both quasars.

Table 1: **ROSAT PSPC Observations of High Redshift Quasars**

Quasar	z^a	$m_V{}^a$	M_V^a	date	obs. ID	wobble	SASS version	exp (sec)	net counts	$N_H{}^b$ (Gal)
S5 0014+81	3.384	16.5	−30.8	1991Mar16-17	rp700083	ON	5_3_2	5951	398	14.4[c]
Q0420−388	3.123	16.9	−30.4	1991Feb20-22	rp700026	OFF	5_3_2	11896	363	1.91[d]
PKS0438−436	2.852	18.8	−28.6	1991Feb19-21	rp700028	OFF	5_3	10725	639	1.5[c]
PKS0438−436				1992Sep19-20	rp700867	ON	6_2	10506	524	1.5[d]
PKS2126−158	3.275	17.3	−30.0	1991May9	rp700025	ON	5_3_2	3424	572	4.85[e]
PKS2126−158				1992Nov12-13	rp700868	ON	6_2	3968	690	4.85[e]
S4 0636+680	3.18	17.2	−30.9	1991Mar16	rp700084	ON	5_2	5342	68	5.7[c]
PKS2000−330	3.78	17.5	−30.3	1991Mar31	rp700080	ON	5_3_2	3740	66	7.5[c]

[a] Veron-Cetty and Veron (1991);

[b] in units of 10^{20} atoms cm^{-2}.

[c] Stark *et al.* (1989).

[e] Heiles and Cleary (1979).

[e] Elvis, Lockman and Wilkes (1989).

Table 2: **PSPC X-ray spectral fits for High Redshift Quasars**

Quasar	fit	$Norm.^a$	α_E	N_H^b	χ^2_ν(dof)	Fe-K EW[c]
S5 0014+81	1	$5.5^{+2.6}_{-1.1}$	$1.07^{+1.2}_{-0.73}$	19^{+24}_{-8}	1.06(18)	<1.1
	2	4.7 ± 0.27	0.82 ± 0.19	14.4 FIXED	1.02(19)	
	3	$5.0^{+2.0}_{-0.6}$	0.92 ± 0.67	64^{+500}_{-64}	1.07(18)	
Q0420−388	1	1.10 ± 0.14	1.27 ± 0.50	$3.6^{+1.7}_{-1.4}$	1.15(18)	<1.4
	2	1.01 ± 0.07	0.73 ± 0.10	1.91 FIXED	1.27(19)	
	3	1.08 ± 0.13	1.24 ± 0.48	34 ± 33	1.17(18)	
PKS0438−436(2/91)	1	$3.6^{+0.8}_{-0.4}$	$0.83^{+0.61}_{-0.35}$	$8.6^{+10.6}_{-3.2}$	1.10(21)	
PKS0438−436(9/92)	1	$2.6^{+0.4}_{-0.3}$	$0.67^{+0.38}_{-0.33}$	$6.5^{+4.8}_{-2.2}$	1.22(21)	
PKS0438−436(tot.)	1	$3.11^{+0.38}_{-0.28}$	$0.70^{+0.27}_{-0.22}$	$6.9^{+3.5}_{-1.8}$	0.47(22)	
	2	2.35 ± 0.08	-0.155 ± 0.06	1.5 FIXED	2.41(23)	
	3	$2.91^{+0.22}_{-0.19}$	0.61 ± 0.22	86^{+49}_{-28}	0.47(22)	<0.78
PKS2126−158(5/91)	1	$10.4^{+3.9}_{-1.6}$	0.52 ± 0.44	11^{+11}_{-4}	1.37(20)	
PKS2126−158(11/92)	1	$12.4^{+5.7}_{-2.2}$	$0.86^{+0.72}_{-0.43}$	$14.8^{+13.2}_{-5.7}$	0.86(20)	
PKS2126−158(tot.)	1	$11.6^{+2.7}_{-1.4}$	$0.70^{+0.41}_{-0.29}$	$12.9^{+7.2}_{-3.8}$	1.03(20)	
	2	8.6 ± 0.3	-0.03 ± 0.07	4.85 FIXED	2.36(21)	
	3	10.3 ± 1.2	$0.52^{+0.25}_{-0.21}$	145^{+120}_{-63}	1.09(20)	0.5 ± 0.5
S4 0636+680	4	1.2 ± 0.3	0.71 FIXED	$590^{+600[d]}_{-340}$	0.82(6)	
PKS2000-330	4	0.9 ± 0.2	0.71 FIXED	$0 + 220^d$	1.53(7)	

[a] in units of 10^{-4} cm^{-2} s^{-1} keV^{-1} @ 1 keV; [b] in units of 10^{20} cm^{-2}; [c] 90% upper limit (keV) for two interesting parameters at 6.4 keV in the emitted frame; [d] absorber in the quasar frame (plus Galactic absorption).

Fit: 1 - z=0 N_H, free; 2 - z=0 N_H, fixed at Galactic HI value; 3 - absorber in the quasar frame, plus absorption fixed at Galactic HI value; 4 - spectral index fixed at the mean value from the fits to the previous four quasars, absorber in the quasar frame, plus absorption fixed at the Galactic HI value.

Table 3: **Fluxes and Luminosities of High Redshift Quasars**

Quasar	fit	f_X^a	L_X^b
S5 0014+81	2	22^{+4}_{-3}	$44^{+3.9}_{-3.4}$
Q0420−388	2	4.8[c]	7.7[c]
PKS0438−436(2/91)	3	14[c]	18[c]
PKS0438−436(9/92)	3	$10^{+2.7}_{-1.4}$	$14^{+2.5}_{-2.1}$
PKS0438−436(total)	3	12[c]	16[c]
PKS2126−158(total)	3	$42^{+9.7}_{-6.6}$	88^{+15}_{-12}
S4 0636+680	4	$5.2^{+1.4}_{-1.4}$	$9.2^{+2.4}_{-2.4}$
PKS2000−330	4	$3.9^{+0.9}_{-0.9}$	$11.7^{+2.7}_{-2.7}$

[a] 0.1-2.5 keV unabsorbed flux in units of 10^{-13} erg cm^{-2} s^{-1} keV^{-1};
[b] 2-10 keV luminosity in units of 10^{46} erg s^{-1} (H_0= 50 km s^{-1} Mpc^{-1}, Ω_0= 0), assuming isotropic emission. The luminosities change by factors of about four for Ω_0=1, depending on each object's redshift.
[c] Wobble off. Systematic uncertainties can be as large as a factor 2, mostly in the direction of the observed fluxes being underestimates.

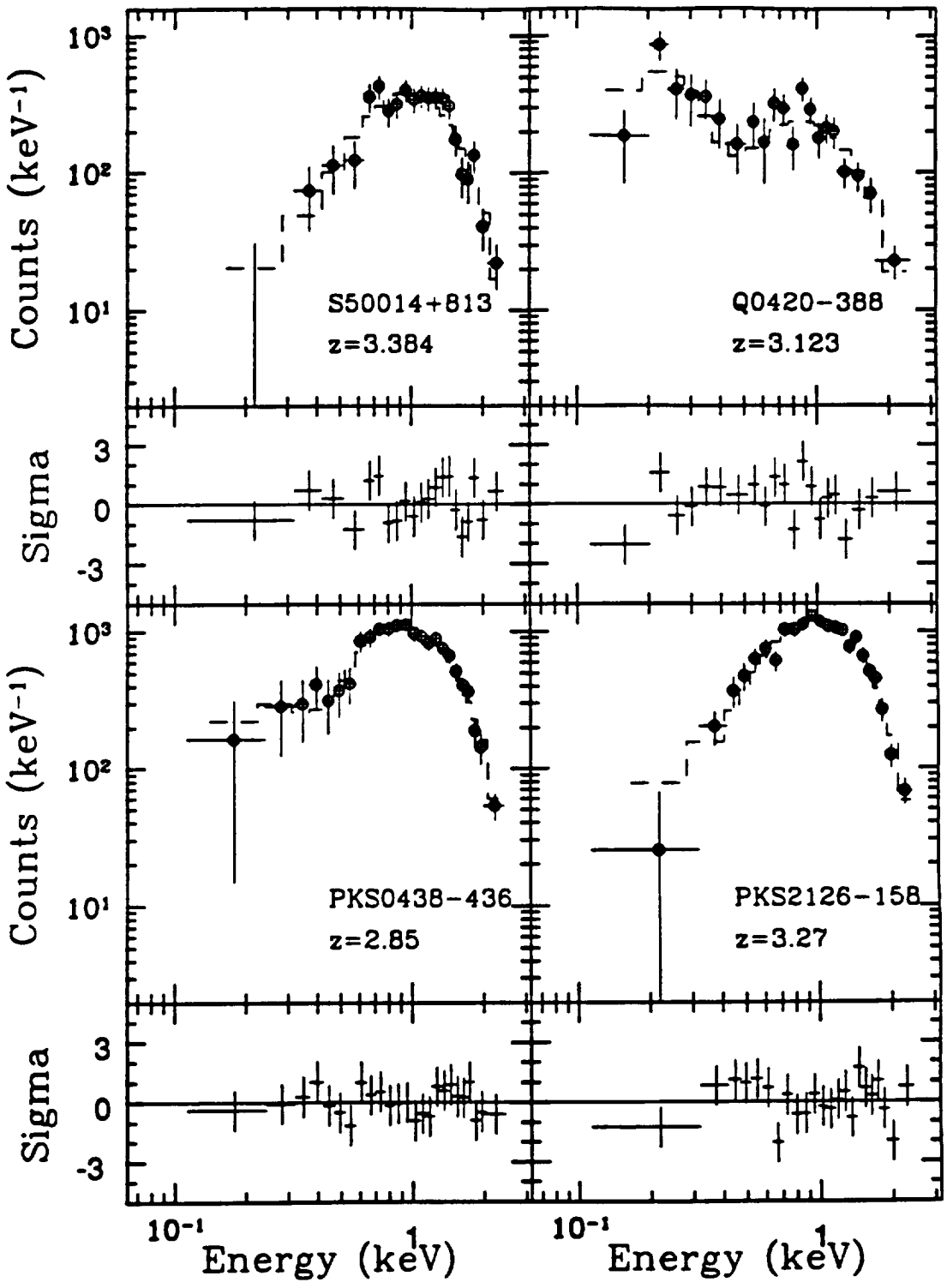
Counts (keV⁻¹)
10³
10²
10¹
S50014+813
z=3.384
Q0420-388
z=3.123
Sigma
3
0
-3
Counts (keV⁻¹)
PKS0438-436
z=2.85
PKS2126-158
z=3.27
Sigma
10⁻¹
1
Energy (keV)
10⁻¹
1
Energy (keV)

Fig. 1

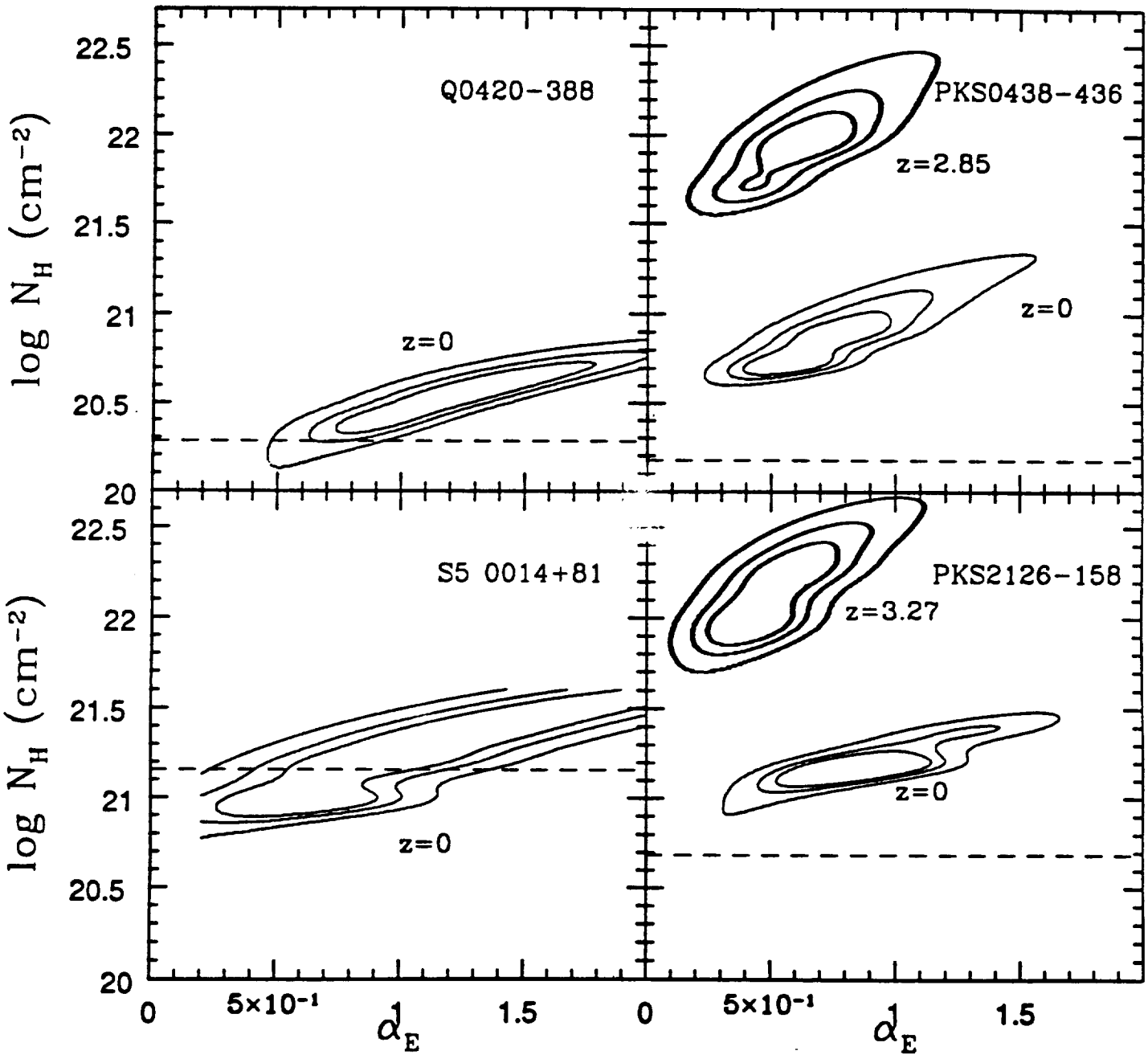
Q0420−388
PKS0438−436
z=2.85
z=0
z=0
S5 0014+81
PKS2126−158
z=3.27
z=0
z=0
log N_H (cm^{-2})
22.5
22
21.5
21
20.5
20
0
5×10⁻¹
1
1.5
α_E

Fig. 2

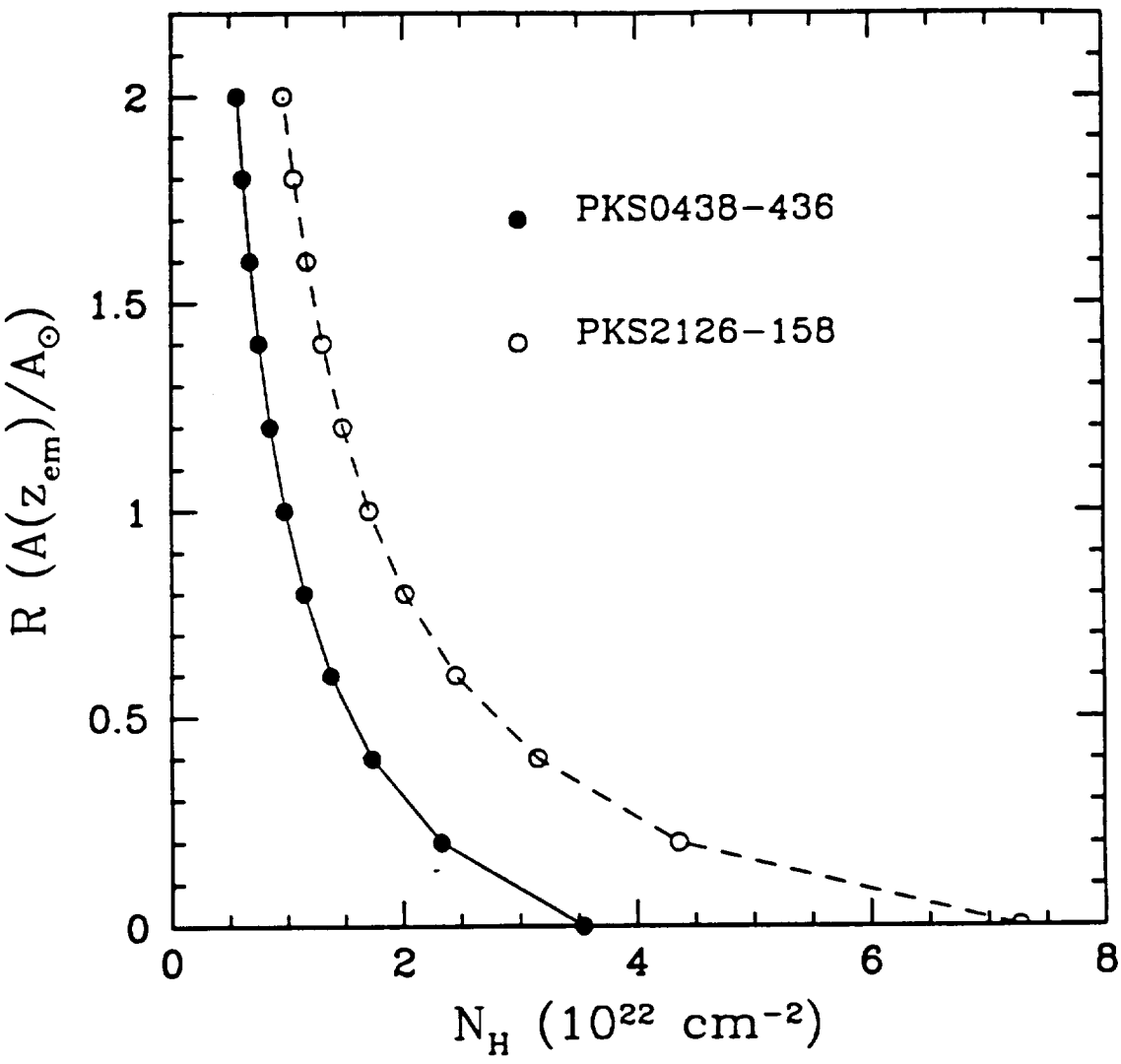

Fig. 3

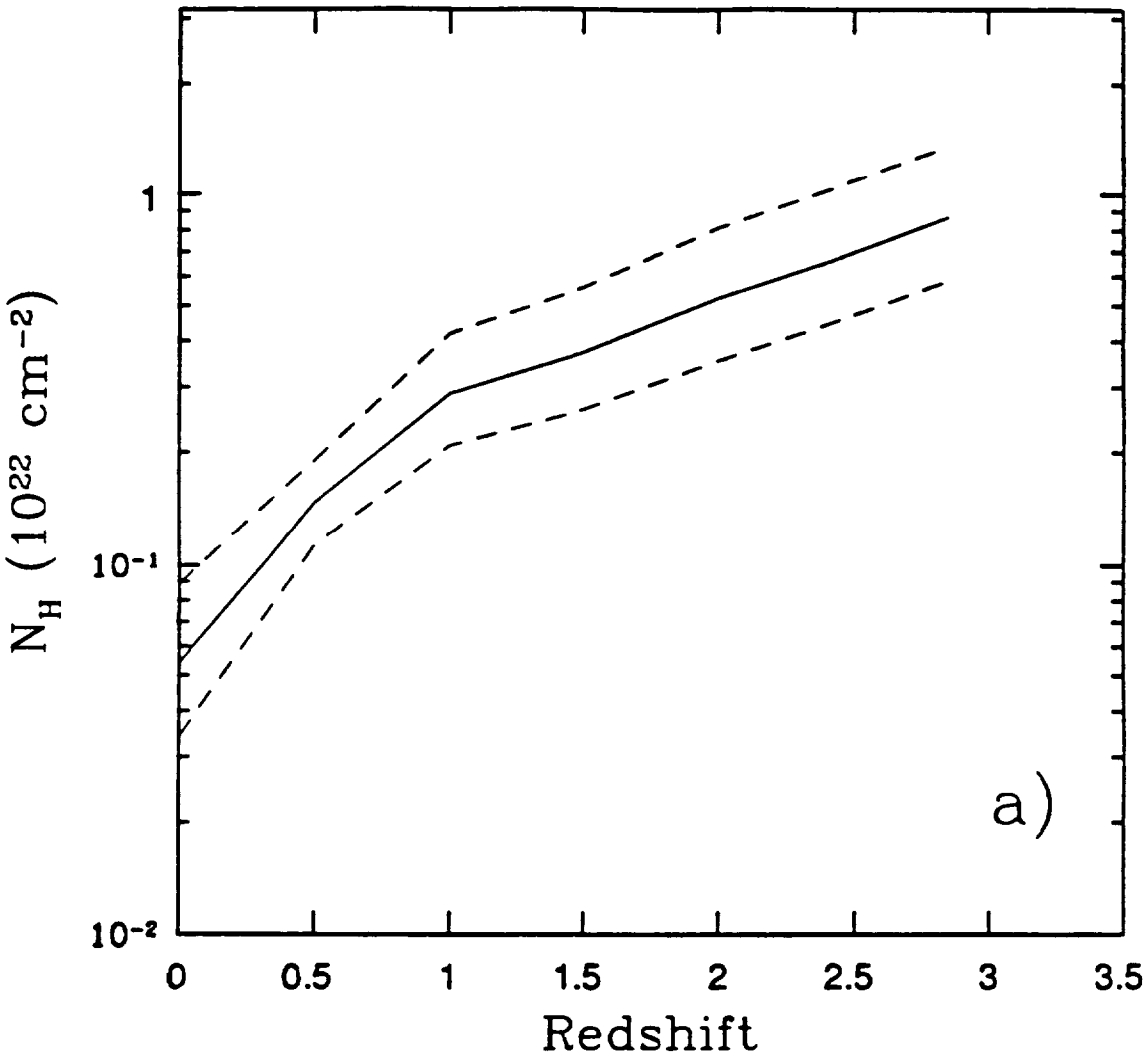

Fig. 4a

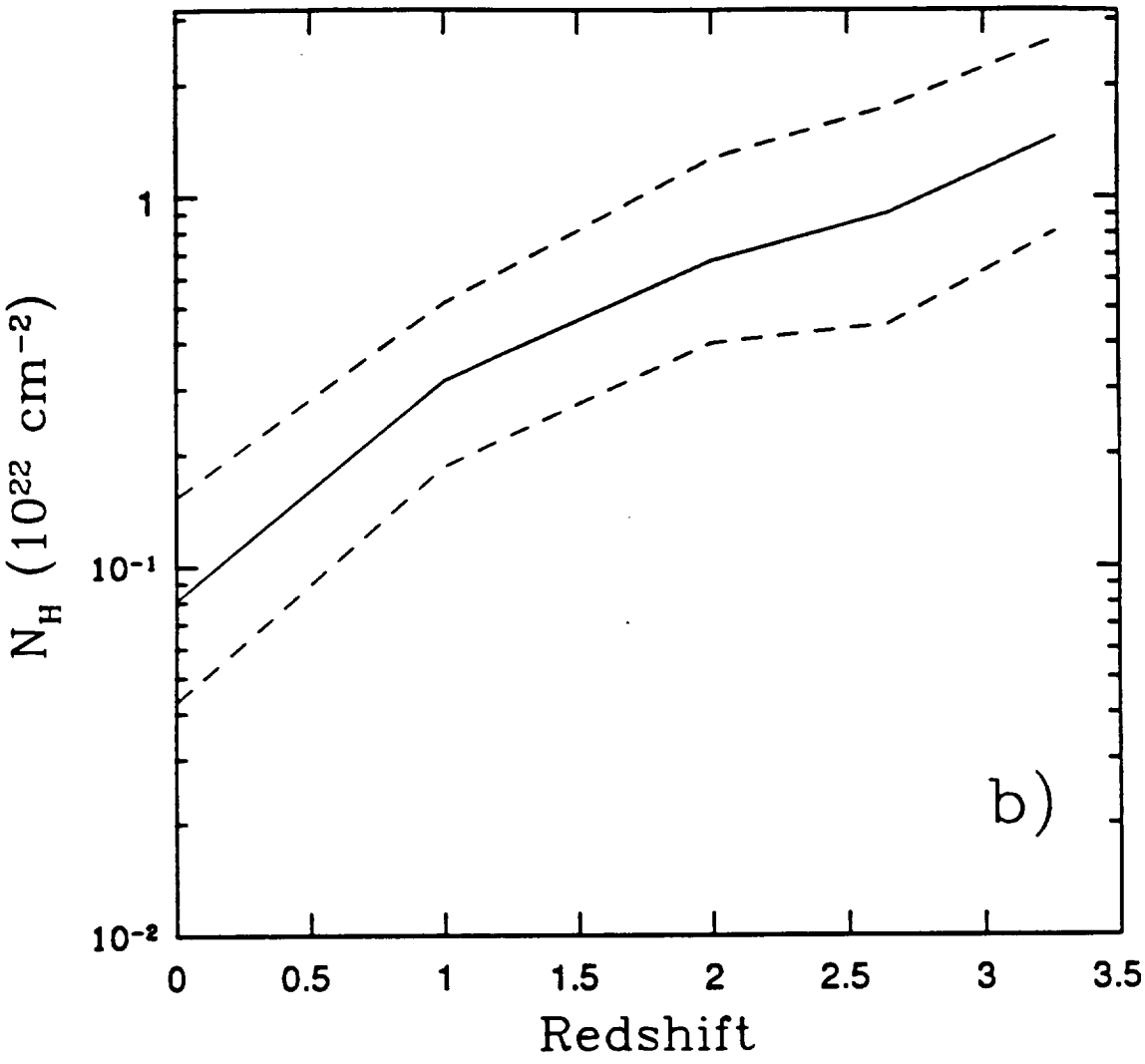

Fig. 4b

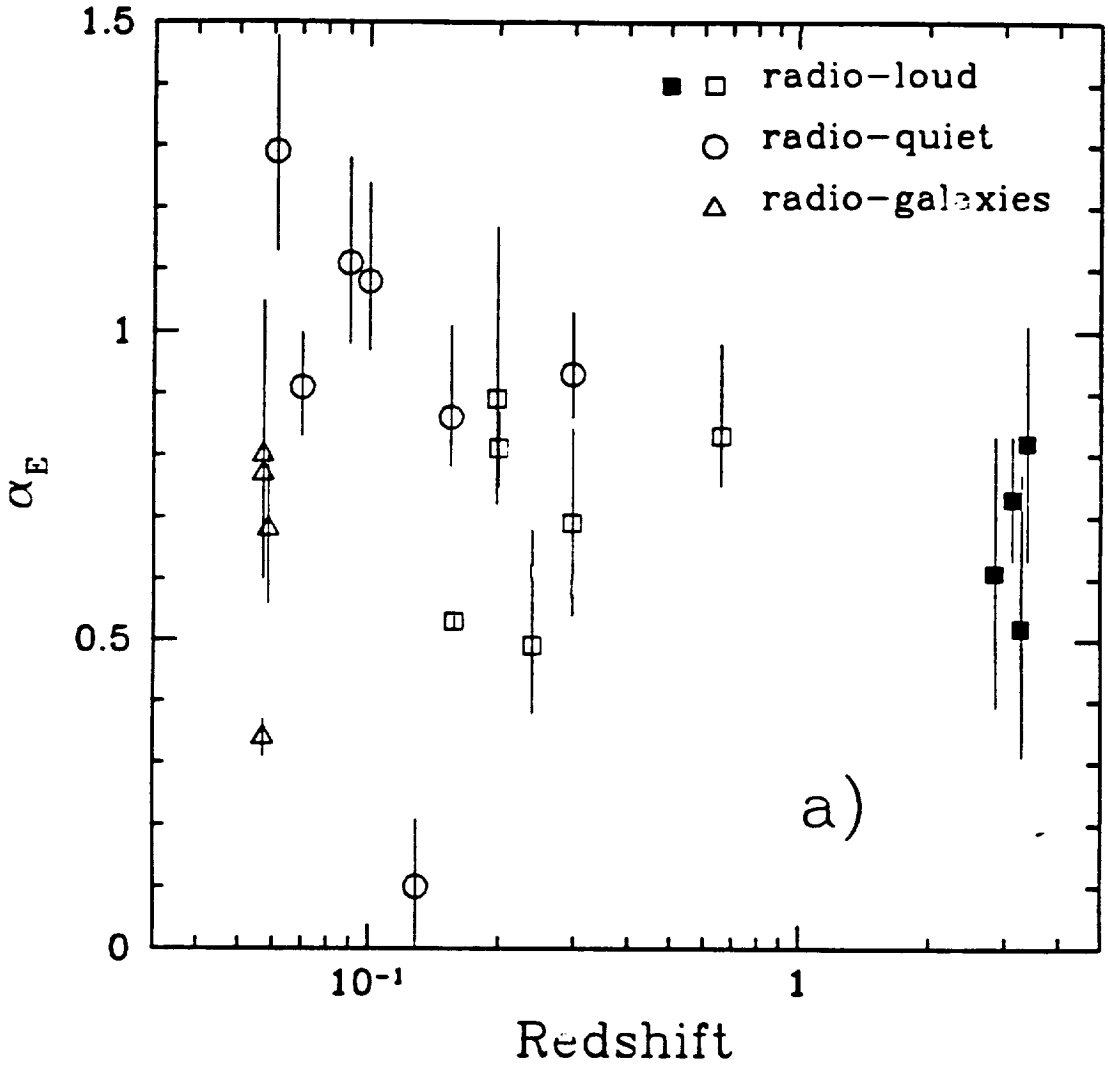
1.5
1
0.5
0
α_E
radio-loud
radio-quiet
radio-galaxies
a)
10^{-1}
1
Redshift

Fig. 5 a

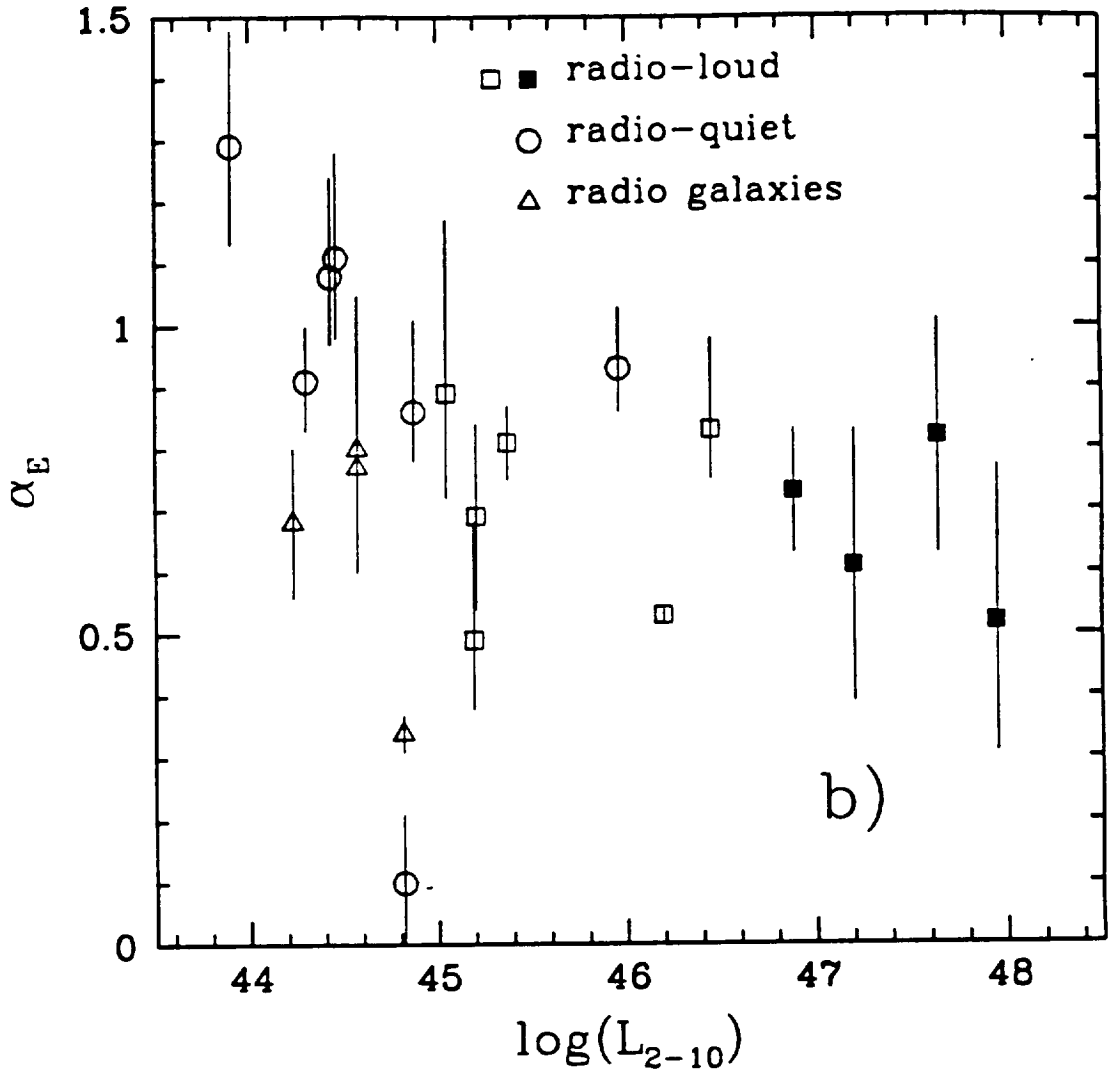
radio-loud
radio-quiet
radio galaxies
b)
1.5
1
0.5
0
α_E
44
45
46
47
48
$\log(L_{2-10})$

Fig. 5b

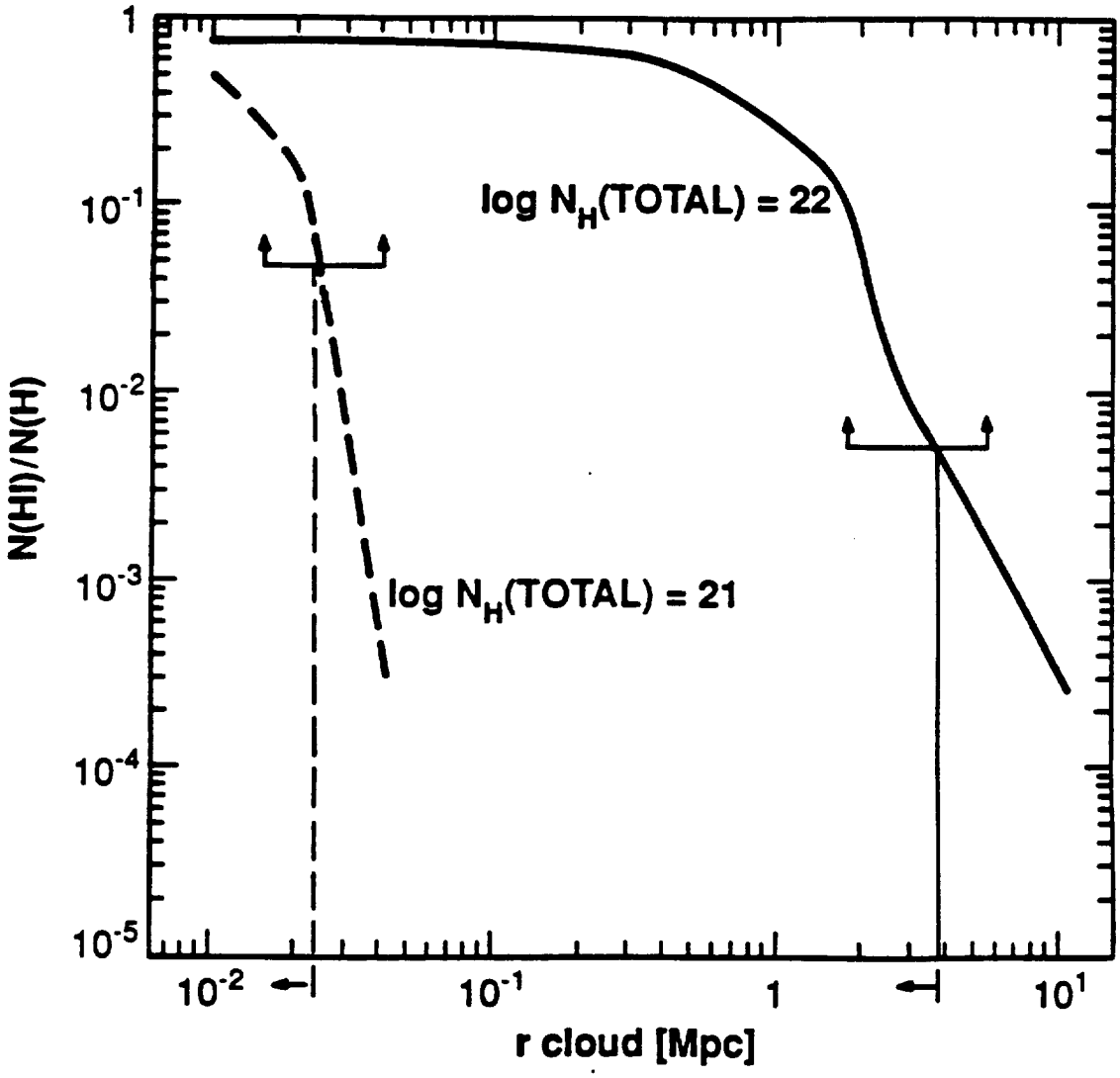
1
10^{-1}
10^{-2}
10^{-3}
10^{-4}
10^{-5}
N(HI)/N(H)
log N_H(TOTAL) = 22
log N_H(TOTAL) = 21
10^{-2}
10^{-1}
1
10^{1}
r cloud [Mpc]

Fig. 6

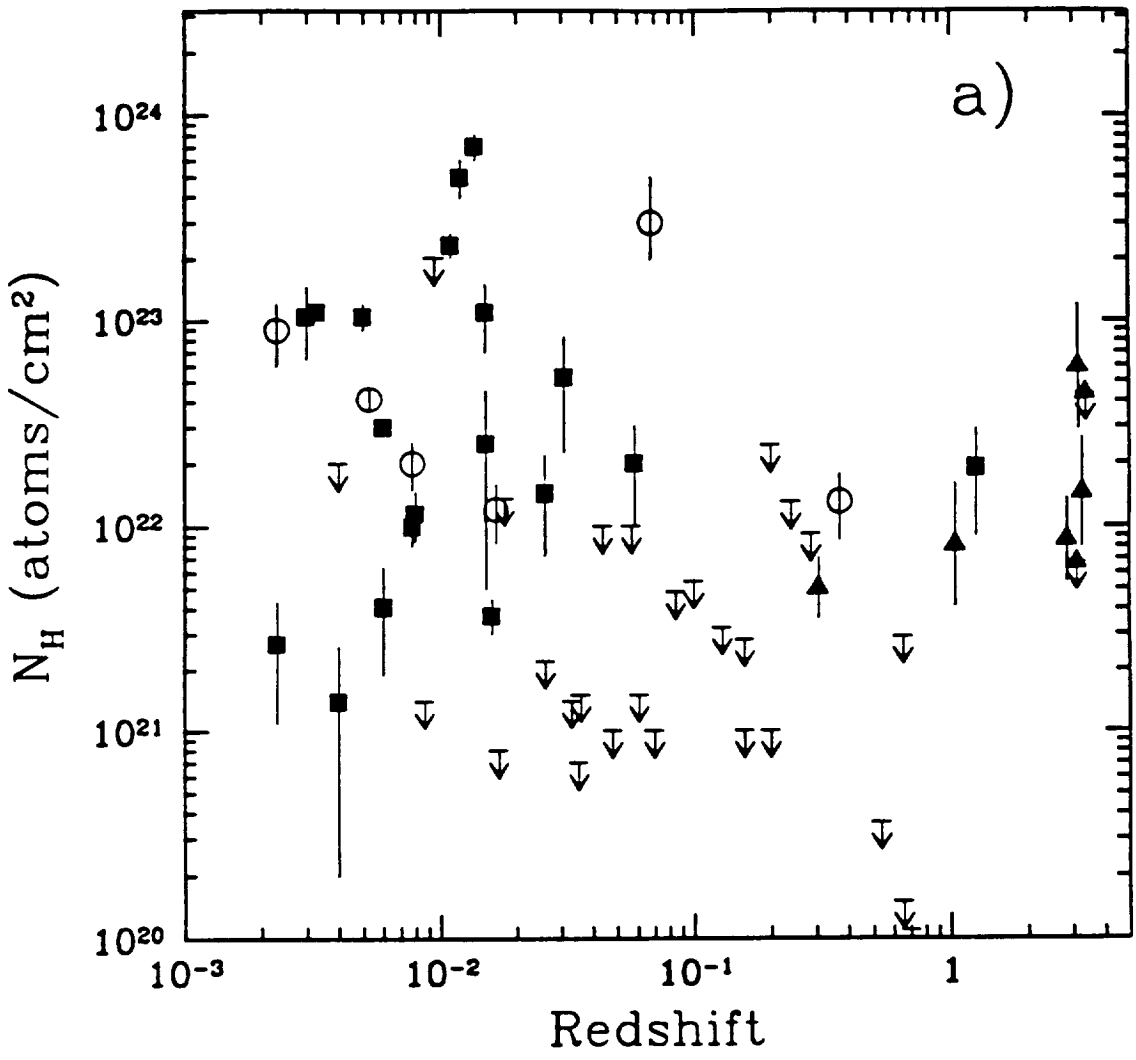

Fig. 7a

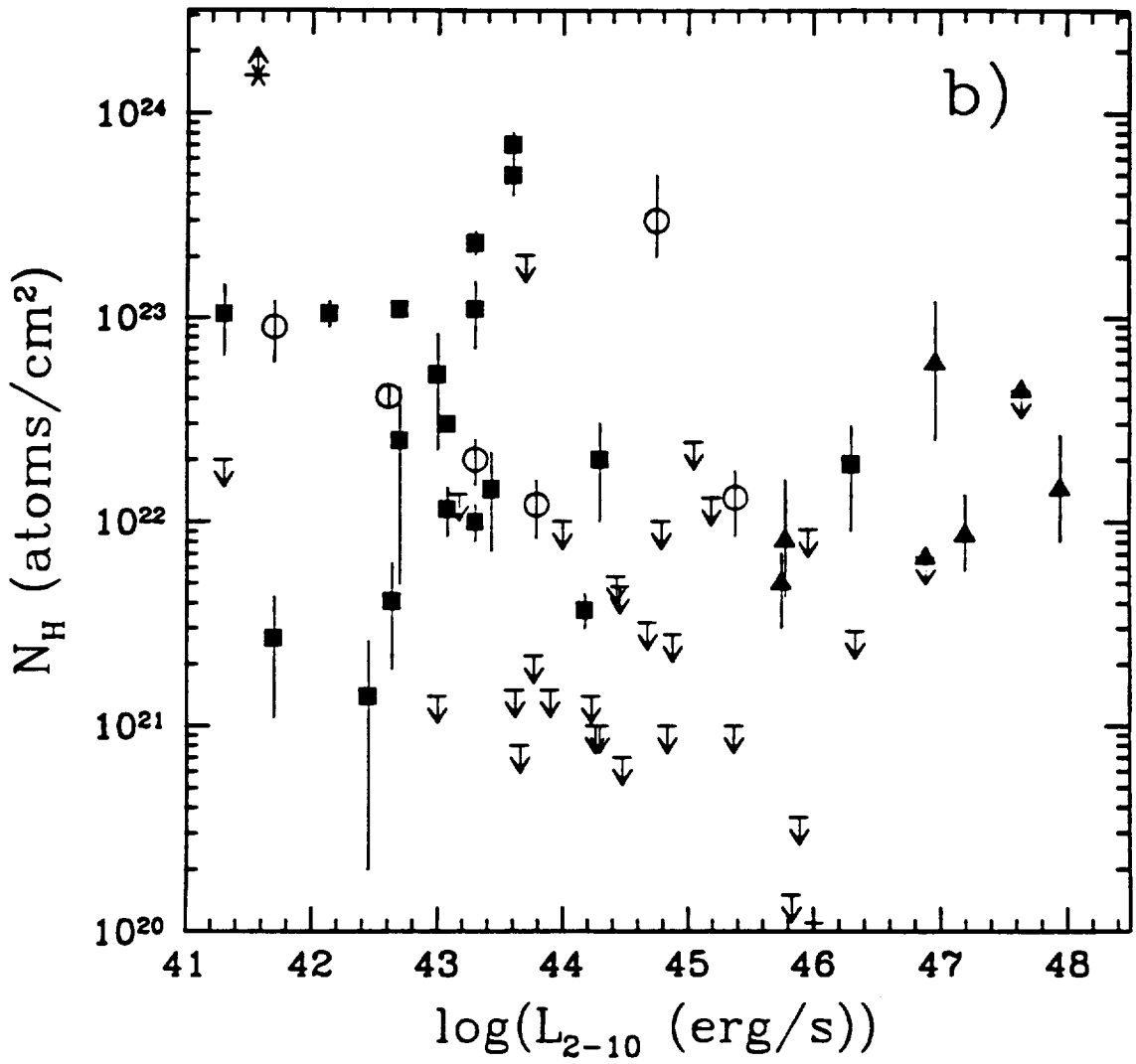
b)
10^{24}
10^{23}
10^{22}
10^{21}
10^{20}
N_H (atoms/cm^2)
41
42
43
44
45
46
47
48
log(L_{2-10} (erg/s))

Fig 7b

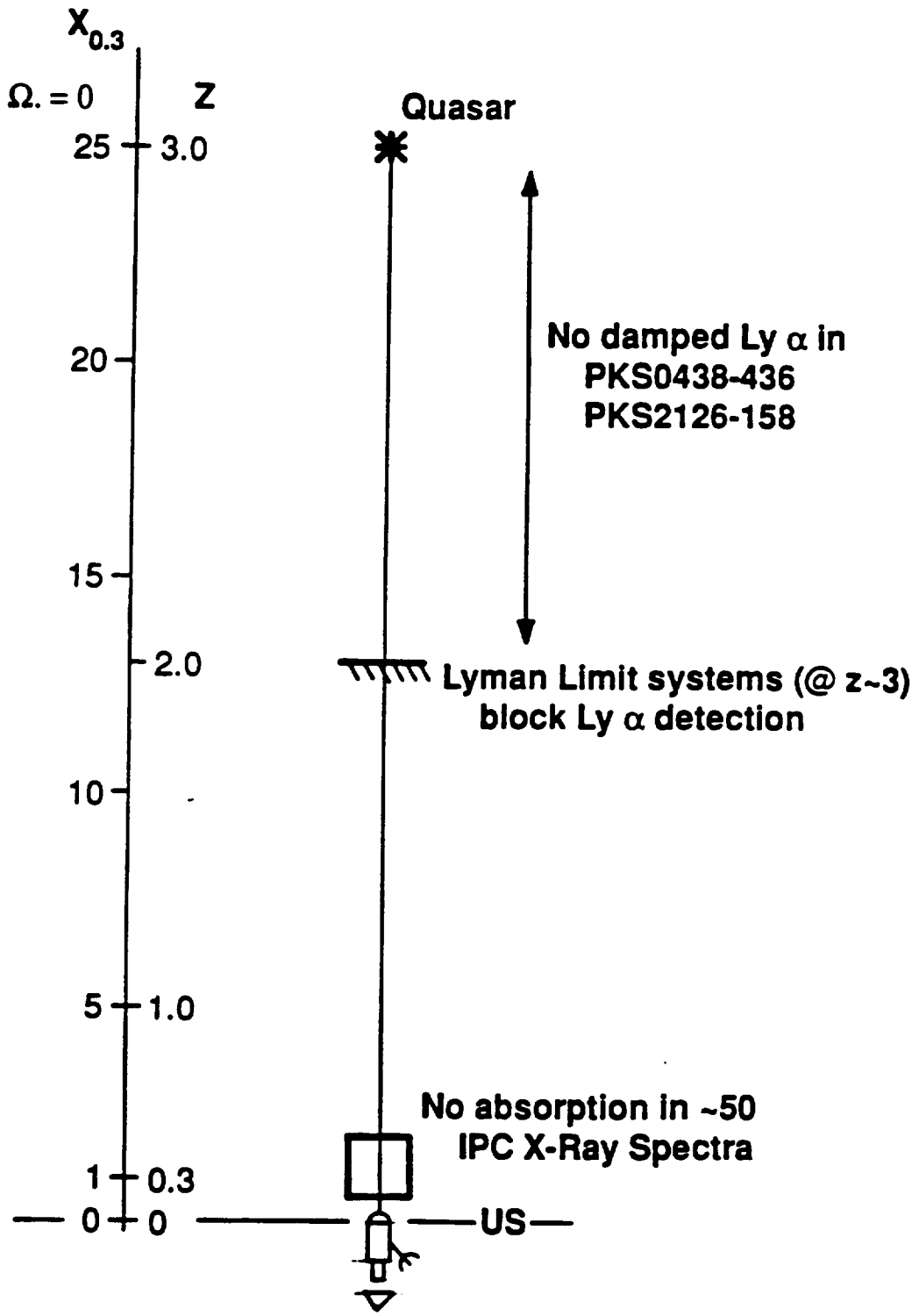
$X_{0.3}$
$\Omega_. = 0$
Z
25
3.0
20
15
2.0
10
5
1.0
1
0.3
0
0
Quasar
No damped Ly α in
PKS0438-436
PKS2126-158
Lyman Limit systems (@ z~3)
block Ly α detection
No absorption in ~50
IPC X-Ray Spectra
US

Fig. 8